AD-A054 678 VERMONT UNIV BURLINGTON DEPT OF CHEMISTRY F/G 7/3
SYNTHESIS, MAGNETIC SUSCEPTIBILITY, AND MOESSBAUER SPECTRA OF F--ETC(U)
MAY 78 J T WROBLESKI, D B BROWN N00014-75-C-0756
UNCLASSIFIED TR-9 NL

| OF |
AD A054678

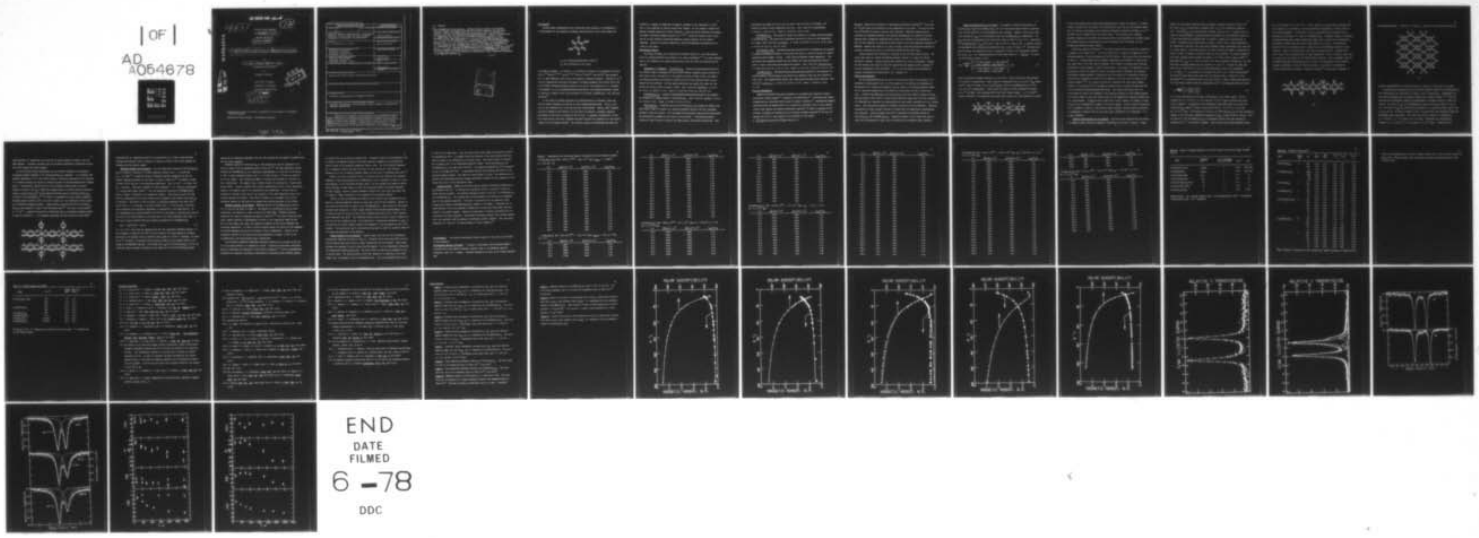

END
DATE FILMED
6 -78
DDC

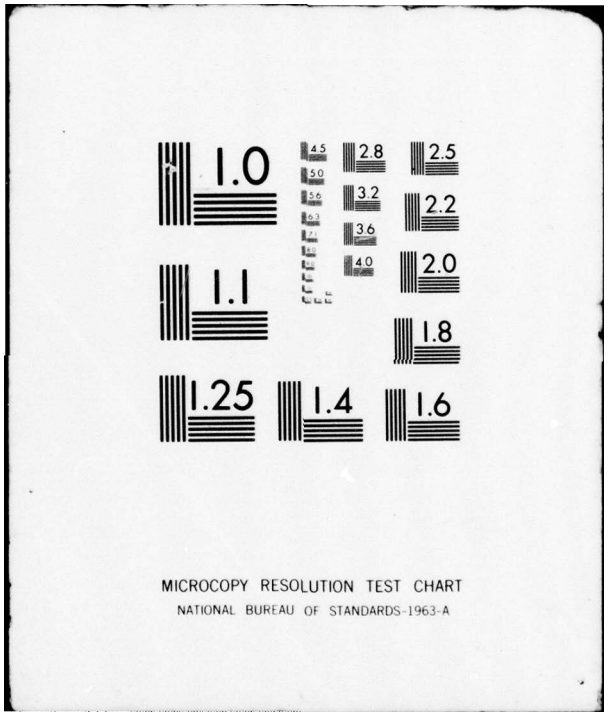
1.0
4.5
5.0
5.6
6.3
2.8
3.2
3.6
4.0
2.5
2.2
2.0
1.8
1.1
1.25
1.4
1.6
MICROCOPY RESOLUTION TEST CHART
NATIONAL BUREAU OF STANDARDS-1963-A

(14) TR-9

(12)

OFFICE OF NAVAL RESEARCH

(15) Contract N00014-75-C-0756

Project .NR 356-593

(9) TECHNICAL REPORT, # 9

(6) Synthesis, Magnetic Susceptibility, and Mössbauer Spectra of Fe(III) Dimers and Fe(II) Polymers Containing 2,5-Dihydroxy-1,4-benzoquinones.

by

(10) James T. Wrobleski and David B. Brown

Prepared for Publication

in

Inorganic Chemistry

University of Vermont

Department of Chemistry

Burlington, Vermont 05401

(11) 22 May 1978

(12) 43p.

408 892

SECURITY CLASSIFICATION OF THIS PAGE *(When Data Entered)*

REPORT DOCUMENTATION PAGE		READ INSTRUCTIONS BEFORE COMPLETING FORM
1. REPORT NUMBER 9	2. GOVT ACCESSION NO.	3. RECIPIENT'S CATALOG NUMBER
4. TITLE *(and Subtitle)* SYNTHESIS, MAGNETIC SUSCEPTIBILITY, AND MÖSSBAUER SPECTRA OF Fe(III) DIMERS AND Fe(II) POLYMERS CONTAINING 2,5-DIHYDROXY-1,4-BENZOQUINONES		5. TYPE OF REPORT & PERIOD COVERED Technical Report
		6. PERFORMING ORG. REPORT NUMBER
7. AUTHOR(s) J. T. Wrobleski, D. B. Brown		8. CONTRACT OR GRANT NUMBER(s) N00014-75-C-0756
9. PERFORMING ORGANIZATION NAME AND ADDRESS Department of Chemistry University of Vermont Burlington, Vermont 05401		10. PROGRAM ELEMENT, PROJECT, TASK AREA & WORK UNIT NUMBERS
11. CONTROLLING OFFICE NAME AND ADDRESS Office of Naval Research Department of the Navy Arlington, Virginia 22217		12. REPORT DATE May 22, 1978
		13. NUMBER OF PAGES 40
14. MONITORING AGENCY NAME & ADDRESS *(if different from Controlling Office)*		15. SECURITY CLASS. *(of this report)* Unclassified
		15a. DECLASSIFICATION/DOWNGRADING SCHEDULE

16. DISTRIBUTION STATEMENT *(of this Report)*

Approved for Public Release, Distribution Unlimited

17. DISTRIBUTION STATEMENT *(of the abstract entered in Block 20, if different from Report)*

18. SUPPLEMENTARY NOTES

Submitted for publication in Inorganic Chemistry

19. KEY WORDS *(Continue on reverse side if necessary and identify by block number)*

dihydroxy benzoquinones, metal polymers, dimers, magnetic susceptibility, Mössbauer spectroscopy

20. ABSTRACT *(Continue on reverse side if necessary and identify by block number)*

Several iron complexes of the dianions of 2,5-dihydroxy-1,4-benzoquinone (DHBQ) and 2, 5-dichloro-3,6-dihydroxy-1,4-benzoquinone (CA, chloranilate dianion) have been prepared and studied by magnetic susceptibility and Mössbauer spectroscopic methods. Iron(II) salts react with these dihydroxybenzoquinones to give polymeric $Fe(DHBQ)(H_2O)_2$ and $Fe(CA)(H_2O)_2$. If the reaction is carried out in the presence of pyrazine, pyr, $[Fe(CA)(pyr)]_n$ →

DD FORM 1 JAN 73 1473 EDITION OF 1 NOV 65 IS OBSOLETE
S/N 0102-014-6601

20. Abstract

and $[Fe(DHBQ)(pyr)]_n$ are obtained. Infrared spectral results are consistent with the presence of bridging bidentate pyr in these complexes, and thus sheet polymers. Dimeric $Fe_2(DHBQ)_3(H_2O)_4$ and $Fe_2(CA)_3(H_2O)_4 \cdot 4H_2O$ are obtained by reacting $FeCl_3$ with the respective dihydroxybenzoquinones. Magnetic susceptibility vs. temperature data obtained for the polymeric materials are fit to a $\underline{S}=2$ Heisenberg linear chain model with $\underline{J} \cong -1.4\ cm^{-1}$ for $[Fe(DHBQ)(H_2O)_2]_n$ and $\underline{J} \cong -2.6\ cm^{-1}$ for $[Fe(DHBQ)(pyr)]_n$. Corresponding values for the CA-containing polymers are $\underline{J} > -0.1\ cm^{-1}$ and $\underline{J} \cong -0.5\ cm^{-1}$, respectively. The Heisenberg-Dirac-Van Vleck $\underline{S}_1=\underline{S}_2=5/2$ spin exchange model applied to the magnetic susceptibility vs. temperature data for $Fe_2(DHBQ)_3(H_2O)_4$ and $Fe_2(CA)_3(H_2O)_4 \cdot 4H_2O$ yields $\underline{J} = -2.0\ cm^{-1}$ and $\underline{J} = -1.0\ cm^{-1}$, respectively. The presence of an anisotropy in the recoilless fraction (Goldanskii-Karyagin effect) is observed in the ^{57}Fe Mössbauer spectra of the Fe(III) dimers and is substantiated by measurements on the temperature dependence of the Mössbauer parameters.

Fe 57

Introduction

Several recent investigations have established that dianions of 2,5-dihydroxy-1,4-benzoquinones (I) are capable of bridging transition-metal ions to form dimers and

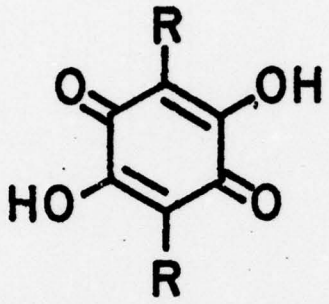

I_a, R=H (dihydroxybenzoquinone, DHBQ H_2)

I_b, R=Cℓ (chloranilic acid, CAH_2)

coordination polymers. For example, 1:1 coordination polymers of the dianion of Ib with Co(II),[1-3] Ni(II),[1,2,4-7] Cu(II),[1,2,7,8] Sn(IV),[9] Pt(II)[10], and Pd(II)[10] were prepared and, in some instances, their optical and magnetic properties measured. Pierpont et al.[11] recently reported the structures and magnetic exchange parameters for several Ni(II) and Cu(II) dimers containing bridging dianions of Ia and Ib with terminal 2,2',2"-triaminotriethylamine, 1,1,4,7,7-pentamethyldiethylenetriamine, and dipropylenetriamine ligands. In addition, a report of the x-ray structure of a Pd dimer, $K_2[PdCℓL]_2$(L = Ib), has also appeared.[12]

In this paper we present syntheses and characterization of polymeric Fe(II) and dimeric Fe(III) complexes of dianions of these dihydroxybenzoquinones. Prior to this work no iron chelates of Ia or Ib had been well characterized. However, Beg[10] prepared an Fe(III) complex of the dianion of Ib for which he proposed a polymeric structure principally on the basis of analytical and ir data. In apparent contradiction to both that report and to this work, Cabbiness and Amis[4] reported the formation of a bis Fe(III) complex of Ib in aqueous solution. Our original purpose in undertaking this study was

primarily to compare the magnitude of magnetic exchange in iron complexes of I with that in iron complexes of similar oxygen donor ligands. We also sought to compare the magnetic exchange exhibited by these compounds to those previously reported for polymers and dimers containing bridging dianions of I.[3,8,11] During the course of this investigation we also observed interesting Mössbauer spectral behavior for the dimeric compounds. Results of variable-temperature, zero-field Mössbauer experiments are included in this paper.

Experimental Section

Both CAH_2 and $DHBQH_2$ were purchased from Eastman Chemical Co. and were purified either by recrystallization from ethanol or by vacuum sublimation.[13] All other compounds used in the syntheses were reagent grade materials and were used as received from the supplier.

Preparation of Complexes. $[Fe(CA)(H_2O)_2]_n$. Polymeric diaquochloranilatoiron(II) was prepared under an atmosphere of N_2 by slowly adding a degassed aqueous solution of $FeSO_4 \cdot 7H_2O$ (1.14g, 4.05 mmole) to a hot aqueous solution of CAH_2 (0.85g, 4.05 mmole). The resulting solution was stirred at reflux for 15 min then quickly cooled to room temperature and filtered. The dark green precipitate was washed with water and then ethanol and finally dried in vacuo at 100°C. Anal. Calcd for $C_6Cl_2FeH_4O_6$: C, 24.11; Cl, 23.73; Fe, 18.69; H, 1.35. Found: C, 23.98; Cl, 23.86; Fe, 18.8; H, 1.22.

$[Fe(DHBQ)(H_2O)_2]_n$. Polymeric diaquodihydroxybenzoquinonatoiron(II) was prepared and isolated in a similar manner to $[Fe(CA)(H_2O)_2]_n$. Anal. Calcd for $C_6FeH_6O_6$: C,31.34; Fe, 24.29; H, 2.63. Found: C, 31.38; Fe, 24.3; H, 2.44.

$[Fe(CA)(pyr)]_n$. A pyrazine analog of $[Fe(CA)(H_2O)_2]_n$ was prepared by adding solid $FeSO_4 \cdot 7H_2O$ (5.64g, 20.3 mmole) to a refluxing methanol solution (250 mL) containing pyrazine (1.63g, 20.3 mmole). The red-orange Fe(II)-pyrazine complex which precipitated was redissolved by adding 25 mL of water to this mixture. A concentrated aqueous solution of CAH_2 (4.24g, 20.3 mmole) was added giving a brown-black precipitate. This

precipitate was washed with 500 mL of hot water, then with 250 mL of ethanol, and finally air dried at room temperature over P_2O_5. Anal. Calcd for $C_{10}Cl_2FeH_4N_2O_4$: C, 35.03; H, 1.18; N, 8.17. Found: C, 34.82; H, 1.02; N, 7.69.

$[Fe(DHBQ)(pyr)]_n$. This pyrazine complex was prepared in a manner exactly analogous to $[Fe(CA)(pyr)]_n$. The brown-black precipitate was dried in vacuo at room temperature over $CaSO_4$. Anal. Calcd for $C_{10}FeH_6N_2O_4$: C, 43.83; Fe, 20.38; H, 2.21; N, 10.22. Found: C, 43.49; Fe, 20.4; H, 2.21; N, 10.62.

$Fe_2(CA)_3(H_2O)_4 \cdot 4H_2O$. Tetraaquotrichloroanilatodiiron(III) tetrahydrate was prepared by adding stoichiometric amounts of $FeCl_3 \cdot 6H_2O$ and CAH_2 to a stirred solution of ethanol containing 10% by weight of water. A dark black precipitate formed immediately. This precipitate was repeatedly washed with hot ethanol and twice recrystallized from hot water to yield a blue-black microcrystalline product. Anal. Calcd for $C_{18}Cl_6Fe_2H_{16}O_{20}$: C, 24.66; Cl, 24.26; Fe, 12.74; H, 1.84. Found: C, 24.71; Cl, 23.58; Fe, 12.6; H, 1.59.

$Fe_2(DHBQ)_3(H_2O)_4$. Tetraquotridihydroxybenzoquinonatodiiron(III) was prepared in a similar manner to $Fe_2(CA)_3(H_2O)_4 \cdot 4H_2O$ except that anhydrous $FeCl_3$ was used instead of $FeCl_3 \cdot 6H_2O$. The recrystallized product was a dark brown microcrystalline material. Anal. Calcd for $C_{18}Fe_2H_{14}O_{16}$: C, 36.15; Fe, 18.68; H, 2.36. Found: C, 35.84; Fe, 18.4; H, 2.23.

Physical Measurements

Magnetic susceptibilities were determined on polycrystalline samples by using a conventional Faraday balance [14] calibrated with $Hg[Co(NCS)_4]$.[15] Corrections for ligand diamagnetism were calculated from a table of Pascal's constants.[16] Experimental magnetic susceptibilities and moments were fit to theoretical expressions with a local computer routine which employs the Simplex minimization algorithm.[17] A number of goodness-of-fit criteria, including the standard error of estimate (standard deviation)[18] and the chi-squared test (eqn 1), were applied to fits obtained in this manner.

$$\chi^2 = \sum_{i=i}^{n} \{[\bar{\chi}_M(obsd)_i - \bar{\chi}_M(calcd)_i]^2 / \bar{\chi}_M(calcd)_i\}/(n-k) \qquad (1)$$

Mössbauer spectra were obtained on a spectrometer previously described.[19] The source was $^{57}Co(Pd)$ which was maintained at room temperature in all cases. A 25 μm α-Fe foil (430 $\mu g\ ^{57}Fe/cm^2$) was used as velocity scale calibrant. Mössbauer spectra were deconvoluted by assuming Lorentzian line contours superimposed on a parabolic baseline. Standard error propagation equations which require the variance in the parameters of best fit were employed to ascertain the error limits on the final Mössbauer parameters.[20] Mössbauer spectra were taken in all cases on finely ground polycrystalline samples dispersed in Vaseline and held in a lead block between Fe-free mylar tape.

Infrared spectra were obtained on a Beckman IR 20A with KBr pressed pellets. TGA curves were taken on a Dupont 900 Thermal Analyzer coupled to a Dupont 950 Thermogravimetric Analyzer. Optical spectra were recorded on a Cary 14 instrument. Spectra of solid samples were taken by using the quantitative KBr pressed pellet technique.[21] Iron was determined by EDTA titrimetry. C, H, N, and Cℓ analyses were performed by Integral Microanalytical Laboratories, Inc., Raleigh, N.C.

Results and Discussion

The following abbreviations are used in this section: DHBQ is the dianion of 2,5-dihydroxy-1,4-benzoquinone (Ia); CA is the dianion of 3,6-dichloro-2,5-dihydroxy-1,4-benzoquinone (Ib, chloranilate dianion); and pyr refers to the neutral pyrazine ligand. The six complexes prepared above are stable for long periods of time if stored over $CaSO_4$. Although $Fe_2(DHBQ)_3(H_2O)_4$ and $Fe_2(CA)_3(H_2O)_4 \cdot 4H_2O$ are slightly soluble in water, DMSO, and CH_3CN we were unable to obtain useful molecular weight data for these compounds. The remaining four complexes are characterized by their marked insolubility in all solvents tested. This insolubility supports a polymeric structure for these materials. Replicate preparations of these polymers resulted in analytically and magnetically indistinguishable materials. Several attempts were made to synthesize the pyridine adducts of $[Fe(CA)(H_2O)_2]_n$ and $[Fe(DHBQ)(H_2O)_2]_n$. Compounds obtained in such cases were very unstable and characterized by rapid loss of pyridine with concomitant metal oxidation.

Magnetic Susceptibility of the Dimers. The magnetic susceptibility behavior of $Fe_2(CA)_3(H_2O)_4 \cdot 4H_2O$ and $Fe_2(DHBQ)_3(H_2O)_4$ over the temperature range 20-300K is characteristic of that expected for antiferromagnetic spin exchange. Figures 1 and 2 show a monotonic decrease in $\bar{\mu}_{eff}$ for $Fe_2(CA)_3(H_2O)_4 \cdot 4H_2O$ and $Fe_2(DHBQ)_3(H_2O)_4$, respectively. The $\bar{\mu}_{eff}$ value for $Fe_2(CA)_3(H_2O)_4 \cdot 4H_2O$ drops from $5.81\mu_B$ at 290K to 4.74 at 21 K. Similarily for $Fe_2(DHBQ)_3(H_2O)_4$, $\bar{\mu}_{eff}$ falls from $5.55\mu_B$ at 290K to $4.04\mu_B$ at 24K. A complete listing of experimental and calculated susceptibility data is given in Table I.[22] Susceptibility data for these two compounds were fit to expression 2 which is the appropriate equation for an $\underline{S}_1 = \underline{S}_2 = 5/2$ Heisenberg-Dirac-Van Vleck dimer model ($H = -2J\hat{\underline{S}}_1 \cdot \hat{\underline{S}}_2$). To obtain the fits shown in Figures 1 and 2

$$\bar{\chi}_M = \frac{2N\beta^2 g^2}{kT} \left[\frac{55 + 30\exp(-10\underline{J}/kT) + 14\exp(-18\underline{J}/kT) + 5\exp(-24\underline{J}/kT) + \exp(-28\underline{J}/kT)}{11 + 9\exp(-10\underline{J}/kT) + 7\exp(-18\underline{J}/kT) + 3\exp(-28\underline{J}/kT) + \exp(-30\underline{J}/kT} \right] + N\alpha \qquad (2)$$

only the isotropic exchange parameter, $\underline{J}$, was varied. Both g and $N\alpha$ were held constant at 2.00 and 0.0 respectively. These values are appropriate for an ion with a $^6\underline{A}_{1g}$ ground term.[23] Best fit values of $\underline{J}$ for $Fe_2(CA)_3(H_2O)_4 \cdot 4H_2O$ and $Fe_2(DHBQ)_3(H_2O)_4$ are -0.95 and -2.00 cm^{-1}, respectively. These values are similar to those obtained by Pierpont et al.[11] for DHBQ - and CA-bridged Ni(II) and Cu(II) dimers (range - 1.1 to $-4.6cm^{-1}$). Dimeric structure II is consistent with these small values of $\underline{J}$. This structure is unique

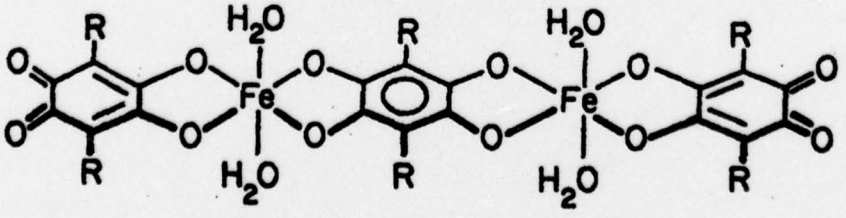

II

in that both bridging and terminal dihydroxybenzoquinone ligands are present. We assume a planar structure for the central core containing the iron ions and the bridging ligand. Such a situation is consistent with structural information obtained by Pierpont et al.[11] for DHBQ- and CA- bridged Ni(II) and Cu(II) dimers. As discussed later, infrared arguments clearly are consistent with chelated rather than monodentate CA and DHBQ ligands. The infrared spectra of these dimers are also consistent with the presence of both bridging and terminal quinone ligands.

Unlike the copper(II) complexes,[11] the Fe(III) ground state is relatively insensitive to changes in the ligand field. It is thus instructive to compare the magnitude of the exchange parameter in several oxygen-donor Fe(III) dimers. Some typical data are presented in Table II. Although quantitative arguments regarding J are difficult to substantiate from these data, it is clear that an increase in the number of bridging atoms increases the barrier to spin exchange in these Fe(III) dimers. By contrast, the magnitude of spin exchange in a series of copper(II) dimers containing oxalate, squarate, and dihydroxybenzoquinone bridges appears to depend more upon the details of the molecular structure (and hence the electronic structure of the copper(II) ion) than upon the nature of the bridging ligand.[11,29] In a series of nickel(II) complexes with these same bridging ligands, it was observed[11] that exchange was smaller with the squarate bridge than with the more extended dihydroxybenzoquinone bridge. This rather surprising result was rationalized in terms of the energies of the available orbitals on the bridging ligands. Our results (Table II) give the reverse order for the magnitude of exchange through these two ligand bridges. In both the Ni(II) and Fe(III) cases, however, the change in ligand bridge is also accompanied by changes in the other ligands. Unless a series of materials can be prepared in which all other factors remain constant, caution should be exhibited in attempting to explain what are relatively small differences in the magnitude of exchange parameters.

Magnetic Susceptibility of the Polymers. Corrected molar susceptibility and effective magnetic moment curves for polymeric $Fe(DHBQ)(H_2O)_2$ are shown in Figure 3. Exper-

imental and calculated susceptibilities and magnetic moments are given in Table I.[22] The value of $\bar{\mu}_{eff}$ is essentially unchanged from 5.6 μ_B in the temperature range 60 - 300K. Below 60K $\bar{\mu}_{eff}$ falls monotonically reaching 3.10μ_B at 10K. It appears that although an antiferromagnetic exchange mechanism dominates the susceptibility behavior at T<~100K, some additional mechanism must be adopted to explain the susceptibility at T>100K. Although the data points shown in Figure 3 result from a single experiment on one preparation, replicate runs using three different sample preparations gave identical ($\pm$ 0.03μ_B) results. These data were fit to several theoretical magnetic susceptibility models in order to propose a structural model for this compound. The axially-symmetric spin-orbit coupling matrix elements of Figgis et al.[30] were used in tabular form[31] to approximate the $\bar{\mu}_{eff}$ vs.. T curve in terms of the orbital reduction parameter k. The term spin-orbit coupling constant was held constant at -100 cm^{-1}. Although the high temperature data ($|kT/\lambda|>0.3$) were fit within experimental error to the parameters $\underset{\sim}{k}$ = 1.0 and $\underline{\nu}$ = -1, no suitable fit was found for $|kT/\lambda| \lesssim 0.3$. Both the Heisenberg[32] and Ising[33] linear chain models were used in fitting the data. Equation 3 is the expression[32] for a Heisenberg chain of $\underline{S}$=2 ions where x = 12$\underline{J}$/kT. Whereas application of the Ising model yielded chemically unreasonable fits,[34] the Heisenberg model was found

$$\bar{\chi} = \frac{2N\beta^2 g^2}{kT}\left(\frac{1 + \coth x - \frac{1}{x}}{1 - \coth x + \frac{1}{x}}\right) \qquad (3)$$

to be a good description of the data, particularily in the T<100K region. The fit obtained for $\underline{J}$ = -1.35 cm^{-1}, g = 2.14, and Nα = 55 x 10^{-6} cgsu is shown as the solid curve in Figure 3. Application of the Heisenberg linear chain model to the data for $[Fe(CA)(H_2O)_2]_n$ (Table I)[22] gave a very good fit for $\underline{J}$ ~ -0.1 cm^{-1}, g = 2.14, and Nα = 55 x 10^{-6} cgsu. The character of this fit for $[Fe(CA)(H_2O)_2]_n$ is not very instructive because of the very small temperature dependence of $\bar{\mu}_{eff}$ (5.8μ_B at 300K to 5.5μ_B at 20K). The value of $\underline{J}$ for $[Fe(DHBQ)(H_2O)_2]_n$ is considerably smaller than that observed by Kobayaski et al.[8] for polymeric Cu(DHBQ). These workers found sample-dependent values

of J in the range -9.7 to -16.7 cm^{-1}. In the absence of a single crystal structure for these polymers it is difficult to attach quantitative significance to these values of the exchange parameter. In addition, we have not satisfactorally accounted for the susceptibility behavior at T > 100K in $[Fe(DHBQ)(H_2O)]_n$. Although a number of situations, including variable chain length polymers and rings, may be invoked for an explanation, experimental evidence does not support these models in this case. An interesting possibility will be discussed later in connection with the Mössbauer spectra of these compounds. There is the possibility that chain terminating Fe(III) - quinone units would account for the susceptibility at high temperatures. Such a situation would result in a lower J but the result is not quantitatively available. Thus the magnetic data for $[Fe(DHBQ)(H_2O)_2]_n$ and $[Fe(CA)(H_2O)_2]_n$ do not allow us to distinguish the two possible polymeric structures, III and IV, from one another. Structure III is favored on intutive grounds and by analogy to reported structures[11] of other metal complexes of

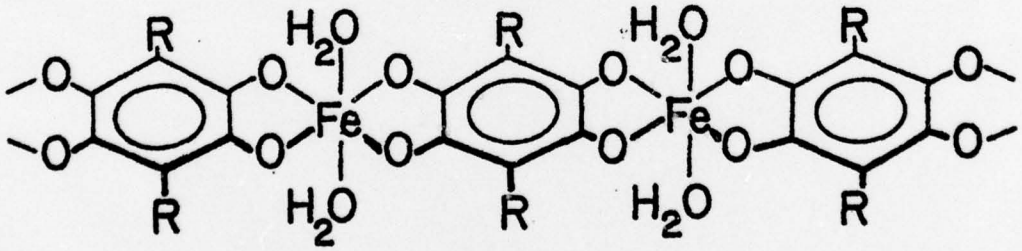

III

dihydroxybenzoquinones. Structure IV, however, is similar to that found for nickel(II)

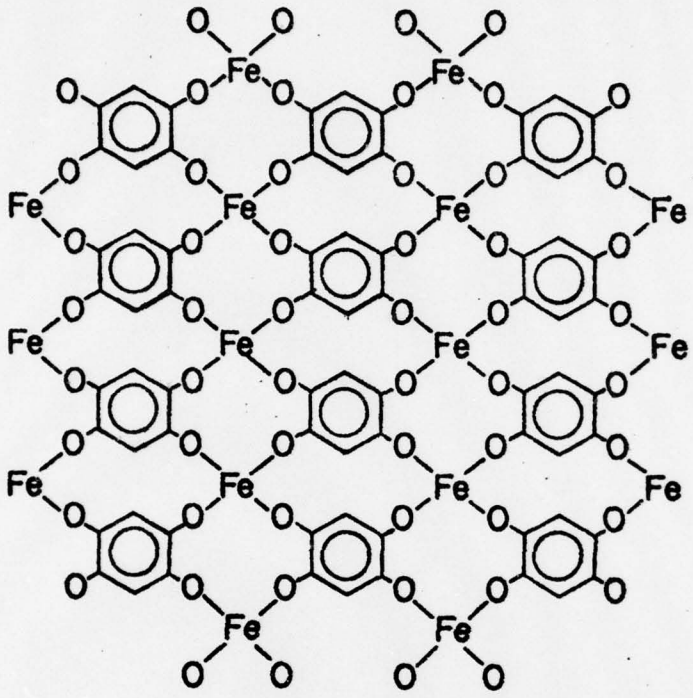

IV

squarate dihydrate,[35] and this structure cannot be ruled out on the basis of our data.

Corrected molar susceptibilities and effective magnetic moments for $[Fe(DHBQ)(pyr)]_n$ and $[Fe(CA)(pyr)]_n$ are illustrated in Figures 4 and 5, respectively. Experimental and calculated susceptibilities and magnetic moments are included in Table I.[22] These two compounds show considerably enhanced antiferromagnetic exchange relative to their aquo analogs. The value of $\bar{\mu}_{eff}$ for $[Fe(DHBQ)(pyr)]_n$ drops from $5.0\mu_B$ at 298K to $2.1\mu_B$ at 12K. The value of $\bar{\mu}_{eff}$ for $[Fe(CA)(pyr)]_n$ decreases at a slower rate from $5.2\mu_B$ at 214K to $4.2\mu_B$ at 14K. As shown in Figures 4 and 5, very good fits were obtained by using the Heisenberg linear chain model. The solid curve shown in Figure 4 is obtained for $\underline{J} = -2.55\ cm^{-1}$, $g = 2.14$, and $N\alpha = 55 \times 10^{-6}$ cgsu. Similarily for $[Fe(CA)(pyr)]_n$ (Figure 5): $\underline{J} = -0.54\ cm^{-1}$, $g = 2.14$, and $N\alpha = 25 \times 10^{-6}$ cgsu. A maximum in the

susceptibility vs. temperature curve near 20K is clearly visible in Figure 4 for the DHBQ compound. As before, replicate data sets showing insignificant differences between them, were obtained for these polymers.

We can envision several explanations for the enhanced exchange in the pyrazine-containing polymers compared to the $[Fe(quinone)(H_2O)_2]_n$ compounds. It is possible that pyrazine complexation to Fe (vide infra) induces a structural preference for III relative to IV thereby lowering the barrier to exchange through the dihydroxybenzoquinone bridging ligand. Alternatively, pyrazine may act as an exchange bridge between Fe centers. Pyrazine is known to act as an effective bridging ligand in several polymeric materials, notably, $[Cu(pyr)_2(NO_3)_2]_n$,[36] $[(bipy)_2ClRu(pyr)[Ru(bipy)_2(pyr)]_n\ RuCl(bipy)_2](PF_6)_{2n+2}\cdot(n+2)H_2O$,[37] and $[COCl_2(pyr)]_n$.[38] The first two compounds are linear chains containing bridging pyrazine molecules while the Co(II) complex is a two dimensional sheet polymer also containing bridging pyrazines. Single-crystal susceptibility data for $[Cu(pyr)_2(NO_3)_2]_n$ were analyzed in terms of the Heisenberg model.[39] The value of $\underline{J}$ was given[39] as -3.7 cm^{-1}. A possible structure for $[Fe(quinone)(pyr)]_n$ containing bridging pyrazine is shown as structure V. It is somewhat surprising that this structure would exhibit

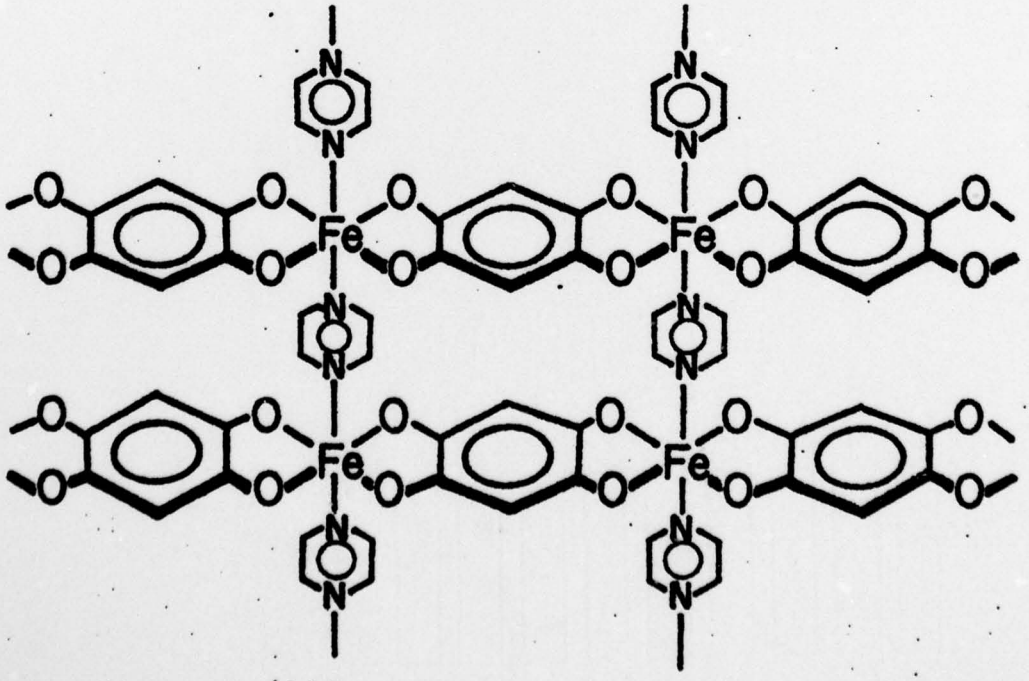

V

susceptibility vs. temperature behavior so characteristic of a linear chain material, although such behavior would be expected if pyrazine provided a more facile pathway for exchange than the quinone ligands.

Mössbauer Spectra of the Polymers. The room temperature spectrum of $[Fe(CA)(H_2O)_2]_n$, shown in Figure 6, consists of a single quadrupole doublet with δ = 1.16 mm/s and ΔE_Q = 2.50 mm/s.[40] A complete listing of Mössbauer spectral parameters for the six quinone complexes discussed in this report is given in Table III.[22] We observe a slight increase in both ΔE_Q and δ with decreasing temperature. Thus, at 15K δ = 1.21 mm/s and ΔE_Q = 2.69 mm/s. Such small increases in these parameters (~ 10 - 20%) are attributable to a second-order Dopper effect.[41] The room temperature spectrum of $[Fe(DHBQ)(H_2O)]_n$, shown in Figure 7, consists of two quadrupole doublets. This spectrum was fit to four lines by constraining the two most intense lines (assigned to the divalent iron site) to be identical. The result of this fit gives the following parameters (see Table III):[22] Fe(II) site, δ = 1.16 and ΔE_Q = 1.47 mm/s; Fe(III) site, δ = 0.38 and ΔE_Q = 0.83 mm/s. These parameters are essentially independent of temperature in the range 300-15K. We have approximated the relative fraction of Fe(III) in the sample by obtaining the ratio of the area of the Fe(III) doublet to the total area of the four Lorentzian lines (eqn. 4). The value of $f_{Fe^{3+}}$ obtained from four different preparations of $[Fe(DHBQ)(H_2O)_2$

$$f_{Fe^{3+}} = A_{Fe^{3+}}/(A_{Fe^{3+}} + A_{Fe^{2+}}) \qquad (4)$$

is 0.14 ± 0.04. This value was obtained from the room temperature Mössbauer spectra. If the assumption is made that the Fe^{3+} sites are required for charge balance at terminal positions in the polymer, then an effective chain length of $11<n<20$ is obtained. We assume the Fe^{3+} is bound to the polymer because extensive washing of the polymer results in no change in its Mössbauer spectrum. We estimate that $f_{Fe^{3+}}$ for $[Fe(CA)(H_2O)_2]_n$ is <0.05. By using this value we obtain an effective chain length of $n>40$ for $[Fe(CA)(H_2O)_2]_n$.These

results are in qualitative agreement with the fits obtained for the magnetic susceptibility data for these compounds.

Mössbauer spectra of $[Fe(CA)(pyr)]_n$ at 295K (spectrum A) and 18K (spectrum B) are shown in Figure 8 and the parameters given in Table III.[22] The high temperature spectra obtained for $[Fe(DHBQ)(pyr)]_n$ are essentially superimposable on those for the CA analog. At 295K, a sharp quadrupole doublet with δ = 1.02 mm/s and ΔE_Q = 2.36 mm/s is observed for the CA complex. Upon cooling the sample to 18K ΔE_Q and δ increase to 3.09 and 1.21 mm/s, respectively. The change in ΔE_Q is rather large to be explained by a second-order Doppler shift. It may be possible that a phase transformation occurs in this temperature range but our magnetic data do not substantiate this possibility. We have found it necessary to include a third line of low intensity in the lower temperature data to adequately describe the spectra. This line is thought to be one member of an Fe(III) quadrupole doublet but our data do not warrant more detailed analysis of this effect.

Mössbauer Spectra of the Dimers. Mössbauer spectra of $Fe_2(DHBQ)_3(H_2O)_4$ taken at 295, 77, and 15K are shown in Figure 9. The spectra of $Fe_2(CA)_3(H_2O)_4 \cdot 4H_2O$ at these temperatures are identical in form to those of the DHBQ dimer. Mössbauer spectral parameters for these two compounds are given in Table III.[22] The value of ΔE_Q for these dimers remains constant at approximately 0.80 mm/s in the temperature range 295-15K. Both of these dimers show large line intensity asymmetry at 295K which decreases with decreasing temperature. In order to study in greater detail the nature of this asymmetry, we obtained Mössbauer spectra of the dimers at several temperatures. Results of the temperature behavior of the spectra are shown graphically in Figures 10 and 11, for $Fe_2(DHBQ)_3(H_2O)_4$ and $Fe_2(CA)_3(H_2O)_4 \cdot 4H_2O$, respectively.

Line intensity asymmetry in Mössbauer hyperfine spectra may be a result of any one of the following factors or a combination of them: crystallite orientation; recoilless fraction anisotropy; and spin-spin or spin-lattice relaxation.[42] We have experimentally eliminated the problem of crystallite orientation by dispersing finely powdered samples

in Vaseline for all the spectra reported here. Relaxation effects are distinguished from the effect of Goldanskii-Karyagin (recoilless fraction) asymmetry by calculating the relative areas of the hyperfine quadrupole doublet lines. For line intensity asymmetry due to relaxation effects the peak area ratio is unity whereas for line intensity asymmetry due to the Goldanskii-Karyagin effect the area ratio is different than unity.[43]

Based on the data in Figures 10 and 11 we believe that the observed line intensity asymmetry in $Fe_2(CA)_3(H_2O)_4{\cdot}4H_2O$ and $Fe_2(DHBQ)_3(H_2O)_4$ may be ascribed, at least to a first approximation, to the Goldanskii-Karyagin effect. We have thusfar been unable to obtain single crystals of these dimers to check the orientation effect and thereby determine the sign of $\underline{e^2qQ}$. However, integral asymmetry coupled with a non unity area ratio does not support a large contribution to the asymmetry from relaxation effects.

Finally, we have investigated the effects on the relative line intensities for the dimers by obtaining Mössbauer spectra by using both thick and thin absorbers. Results of this study are also shown in Figure 10 for $Fe_2(DHBQ)_3(H_2O)_4$. Open circles in this figure represent data taken with a "thick" random absorber which contained approximately 25 mg of natural Fe per cm^2 while the full circles represent data taken with a "thin" absorber which contained 8 mg Fe/cm^2. The difference between these two sets of data is significant only for the line intensity ratio. Thus essentially no temperature dependence of $\underline{I_2}/\underline{I_1}$ is observed for the "thick" absorber whereas the asymmetry is very pronounced for the "thin" absorber. This observation may be qualitatively explained in terms of saturation effects[44] involving self-absorption in the absorber.

Thermal Analysis of the Complexes. Thermal weight loss data for the Fe-dihydroxybenzoquinone complexes are given in Table IV. Processes which occur below 250°C are well defined whereas those which occur at higher temperatures are very diffuse. These former processes are assigned to loss of water from the samples. Two low temperature inflections are observed for $Fe_2(CA)_3(H_2O)_4{\cdot}4H_2O$. The first occurs at 100°C and is assigned to loss of lattice water. The second occurs at 220°C and, because it is identical to the 100°C weight loss, is assigned to loss of coordinated water. Loss of coordinated water occurs

at 240°C for the DHBQ dimer. Both the dimers shown broad weight loss profiles centered at approximately 375°C. No organic matter was detected in the final residue which was shown by powder x-ray diffraction to be mainly Fe_2O_3. This final process is therefore due to gradual loss of the dihydroxybenzoquinone ligand. Both $[Fe(CA)(H_2O)_2]_n$ and $[Fe(DHBQ)(H_2O)_2]_n$ lose water near 240-250°C. Only gradual decomposition of the material occurs in the range 280-550°C. A complicated process occurs between 280-480°C for the pyrazine-bridged polymers. Here again the final product is Fe_2O_3. The combined loss of pyrazine and dihydroxybenzoquinone ligands undoubtedly accounts for the complexity of the weight loss curve in this temperature range.

Infrared Spectra. $DHBQH_2$ and CAH_2 both display carbonyl stretching frequencies at approximately 1650 cm^{-1}. As expected this absorption shifts to 1500 cm^{-1} in both the dimers and aquo polymers. The carbonyl absorption shifts to 1540 cm^{-1} in $[Fe(CA)(pyr)]_n$ and $[Fe(DHBQ)(pyr)]_n$. The carbonyl band is much broader in the dimeric iron complexes than in the polymeric materials. This fact is consistent with the presence of both bridging and terminal dihydroxybenzoquinone ligands in the dimers. In general the infrared spectra of the iron complexes of DHBQ and CA contain many fewer bands than the spectra of the parent ligands. Absence of these bands is entirely consistent with our formulation for these compounds. The pyrazine-containing polymers have infrared spectra which are consistent with the presence of bidentate pyrazine ligands. Thus, the ν(pyr) absorption at ~ 1600 cm^{-1} is entirely absent in these compounds.[44]

Acknowledgment. The authors acknowledge financial support of this work by the Office of Naval Research.

Supplementary Material Available: A listing of experimental and calculated magnetic susceptibilities and effective magnetic moments, Table I, and Mössbauer spectral parameters, Table III (8 pages). Ordering information is given on any current masthead page.

Table I . Experimental and Calculated Magnetic Susceptibilities and Effective Moments

$Fe_2(CA)_3(H_2O)_4 \cdot 4H_2O$: MWt = 876.75, $\chi^{corr} = -365 \times 10^{-6}$ cgsu, $J_{dimer} = -0.95 cm^{-1}$, g = 2.00, Nα = 0.0.

T,K	$\bar{\chi}_M'$(obsd) x 10^5	$\bar{\chi}_M$(calcd) x 10^5	$\bar{\mu}_{eff}$/Fe,μ_B
21.2	26530	26620	4.74
21.9	26300	26140	4.80
24.3	24950	24650	4.93
26.4	23320	23470	4.96
28.9	22040	22150	5.05
47.1	15370	15440	5.38
53.4	14050	13960	5.48
59.6	12660	12720	5.49
59.7	12620	12700	5.49
73.1	10510	10670	5.54
85.9	9036	9245	5.57
101.0	7867	7979	5.64
109.9	7264	7382	5.65
113.2	7113	7187	5.67
128.6	6265	6382	5.68
144.6	5624	5717	5.70
156.2	5228	5318	5.71
161.8	5115	5144	5.75
182.1	4588	4596	5.78
207.4	4060	4057	5.80
232.0	3626	3642	5.80
291.5	2891	2920	5.81

$Fe_2(DHBQ)_3(H_2O)_4$: MWt = 598.00, $\chi^{corr} = -229 \times 10^{-6}$ cgsu, $J_{dimer} = -2.00$, g = 2.00, Nα = 0.0.

T,K	$\bar{\chi}_M^1$(obsd) x 10^5	$\bar{\chi}_M$(calcd) x 10^5	$\bar{\mu}_{eff}$/Fe,μ_B
24.3	16810	15740	4.04
24.9	16550	15670	4.06
26.1	15980	15520	4.08
26.9	15900	15410	4.14
28.3	15820	15220	4.20

T,K	$\bar{\chi}_M^{-1}$(obsd) x 10^5	$\bar{\chi}_M$(calcd) x 10^5	$\bar{\mu}_{eff}$/Fe,μ_B
29.5	15150	15040	4.23
31.4	14620	14750	4.28
33.7	14180	14390	4.37
35.2	13940	14150	4.43
36.2	13480	13990	4.42
39.9	12820	13400	4.52
44.7	11950	12660	4.62
45.8	11780	12500	4.64
49.8	11380	11930	4.76
53.9	10830	11390	4.83
56.4	10530	11060	4.88
66.0	9363	9977	4.97
68.5	9109	9716	5.00
80.2	8027	8666	5.07
93.8	7052	7683	5.14
104.6	6394	7035	5.17
108.2	6097	6843	5.14
125.4	5461	6050	5.23
148.6	4740	5226	5.31
171.9	4104	4596	5.31
222.1	3362	3644	5.46
292.7	2630	2820	5.55

$[Fe(CA)(H_2O)_2]_n$: MWt = 298.86, χ^{corr} = -95.4 x 10^{-6} cgsu, $\underline{J}$ = -0.06 cm^{-1}, g = 2.18, $N\alpha$ = 45 x 10^{-6} cgsu.

T,K	$\bar{\chi}_M^{-1}$(obsd) x 10^5	$\bar{\chi}_M^{-1}$(calcd) x 10^5	$\bar{\mu}_{eff}$/Fe,μ_B
20.3	18750	18680	5.52
21.1	18210	18000	5.55
21.9	17580	17420	5.54
23.0	16580	16600	5.52
24.3	15610	15700	5.51
26.3	14310	14550	5.49
28.4	13210	13520	5.48
33.9	11320	11360	5.54
37.8	10370	10220	5.60

T,K	$\bar{\chi}_M^{-1}$(obsd) x 10^5	$\bar{\chi}_M^{-1}$(calcd) x 10^5	$\bar{\mu}_{eff}$/Fe,μ_B
40.8	9376	9477	5.53
46.3	8278	8375	5.54
60.0	6465	6487	5.57
69.0	5666	5643	5.59
82.4	4753	4739	5.60
99.5	3993	3929	5.64
123.2	3259	3178	5.67
127.1	3150	3082	5.66
132.5	3016	2957	5.65
135.8	2972	2885	5.68
139.1	2882	2817	5.66
158.3	2684	2478	5.83
172.5	2401	2275	5.76
184.0	2245	2134	5.75
204.3	2056	2023	5.80
226.4	1834	1736	5.76

$[Fe(DHBQ)(H_2O)_2]_n$: MWt = 229.96, χ^{corr} = - 85 x 10^{-6} cgsu, J_H = - 1.35, g = 2.14, Nα = 55 x 10^{-6} cgsu.

T,K	$\bar{\chi}_M^{-1}$(obsd) x 10^5	$\bar{\chi}_M$(calcd) x 10^5	$\bar{\mu}_{eff}$/Fe,μ_B
10.3	11730	11930	3.10
11.2	11910	11940	3.27
13.6	11550	11831	3.54
16.1	11500	11550	3.85
20.0	11000	10940	4.20
20.9	10880	10790	4.27
24.3	10160	10210	4.44
27.0	10070	9750	4.67
30.0	9192	9265	4.70
34.7	8979	8564	4.99
38.0	8407	8124	5.05
42.7	7748	7547	5.15
46.2	7485	7168	5.26
49.5	7051	6843	5.28
52.0	6904	6605	5.36

T,K	$\bar{\chi}_M^{-1}$(obsd) x 10^5	$\bar{\chi}_M$(calcd) x 10^5	$\bar{\mu}_{eff}$/Fe,μ_B
54.9	6765	6354	5.45
59.3	6170	6008	5.41
65.0	5594	5609	5.39
67.6	5446	5438	5.43
72.3	5003	5165	5.38
75.5	4948	4991	5.46
81.8	4625	4675	5.50
86.4	4247	4474	5.42
94.9	4136	4136	5.60
99.1	3901	3990	5.56
106.7	3689	3746	5.61
111.2	3463	3615	5.55
117.5	3338	3447	5.60
126.2	3061	3238	5.56
133.5	2886	3081	5.55
141.7	2697	2924	5.53
147.8	2600	2815	5.54
163.0	2365	2577	5.55
167.6	2310	2513	5.56
174.3	2217	2424	5.56
181.2	2134	2340	5.56
191.8	2010	2220	5.55
195.7	1977	2180	5.56
203.8	1899	2100	5.56
211.7	1821	2027	5.55
216.7	1784	1983	5.56
230.0	1696	1876	5.58
236.2	1636	1830	5.56
241.4	1595	1793	5.55
254.3	1525	1708	5.57
257.8	1512	1686	5.58
265.7	1461	1639	5.57
257.3	1419	1584	5.59
283.6	1373	1540	5.61
292.5	1313	1495	5.54
293.8	1332	1490	5.59

$[Fe(CA)(pyr)]_n$: MWt = 342.91, χ^{corr} = - 139.2 x 10^{-6} cgsu, $\underline{J}_H$ = -0.54 cm^{-1}, g = 2.14, $N\alpha$ = 25 x 10^{-6} cgsu.

T,K	$\bar{\chi}^{-1}_M$(obsd) x 10^5	$\bar{\chi}_M$(calcd) x 10^5	$\bar{\mu}_{eff}$/Fe,μ_B
14.0	15510	15710	4.17
14.8	14920	15210	4.20
17.8	13990	13560	4.47
18.9	13400	13050	4.49
20.6	12520	12290	4.54
22.5	11460	11520	4.55
26.2	10230	10300	4.63
28.9	9438	9547	4.67
31.3	8770	8951	4.69
35.5	7988	8090	4.76
40.0	7240	7320	4.81
44.1	6699	6735	4.86
49.7	6031	6071	4.90
53.9	5606	5659	4.91
56.5	5410	5423	4.94
66.3	4650	4701	4.96
71.8	4363	4369	5.00
76.5	4121	4121	5.02
80.0	3948	3956	5.03
86.1	3684	3695	5.04
96.7	3315	3319	5.06
103.1	3120	3125	5.07
109.8	2947	2945	5.09
117.1	2786	2771	5.11
123.7	2648	2631	5.12
129.7	2533	2514	5.13
149.3	2234	2199	5.16
157.3	2118	2091	5.16
165.0	2026	1997	5.17
170.3	1957	1937	5.16
176.6	1900	1871	5.18
182.2	1842	1816	5.18
188.4	1785	1758	5.19
193.9	1739	1710	5.19

T,K	$\bar{\chi}_M^{-1}$(obsd) x 10^5	$\bar{\chi}_M$(calcd) x 10^5	$\bar{\mu}_{eff}$/Fe,μ_B
200.1	1681	1658	5.19
207.1	1635	1604	5.20
212.7	1601	1562	5.22
213.9	1578	1554	5.20

$[Fe(DHBQ)(pyr)]_n$: MWt = 274.02, χ^{corr} = -125 x 10^{-6} cgsu, J_H = - 2.55 cm^{-1}, g = 2.14, $N\alpha$ = 55 x 10^{-6} cgsu.

T,K	$\bar{\chi}_M^{-1}$(obsd) x 10^5	$\bar{\chi}_M$(calcd) x 10^5	$\bar{\mu}_{eff}$/Fe,μ_B
12.6	4510	4514	2.13
14.2	4580	4577	2.28
19.8	4700	4691	2.73
24.6	4666	4667	3.03
38.7	4271	4269	3.64
49.1	3896	3897	3.91
60.2	3525	3526	4.12
81.8	2938	2937	4.38
102.2	2520	2521	4.54
122.9	2198	2198	4.65
153.6	1840	1843	4.75
181.2	1609	1608	4.83
200.9	1472	1473	4.86
210.7	1410	1413	4.87
221.5	1356	1353	4.90
246.8	1230	1231	4.93
259.1	1180	1179	4.95
275.3	1116	1116	4.96
298.4	1039	1038	4.98

Table II. Magnetic Exchange Parameters for Fe(III) Dimers with Various Oxygen Bridging Units.[a]

Compd	Bridging Unit	No. of bridging Units per Dimer	J, cm^{-1}	Ref
$Fe_2(CA)_3(H_2O)_4 \cdot 4H_2O$	$C_6Cl_2O_4$	1	-0.95	this work
$Fe_2(DHBQ)_3(H_2O)_4$	$C_6H_2O_4$	1	-2.00	this work
$[Fe_2(Sq)(phen)_4]Cl_4$	C_4O_4	1	-3.2	24
$[Fe_2(Ox)(phen)_4]Cl_4$	C_2O_4	1	-6.8	24
$[Fe(Sq)(OH)(H_2O)_2]_2 \cdot 2H_2O$	OH	2	-6.9	25
$[Fe(Dipic)(OH)(H_2O)]_2$	OH	2	-11.4	26
$\{[Fe(bipy)_2]_2O\}Cl_4$	O	1	-105	27,28

[a]Abbreviations: Sq = squarate dianion; phen = 1,10-phenanthroline; Dipic = 2,6-pyridine-dicarboxylate; bipy = 2,2 - bipyridine.

Table III. Mössbauer Parameters [a]

Compd	mg Fe / cm^2	T,K	δ, mm/s	ΔE_Q, mm/s	Γ_2/Γ_1 [b]	A_2/A_1 [c]	I_2/I_1 [d]
$[Fe(CA)(H_2O)_2]_n$	8	295	1.16	2.50	1.03	1.07	1.05
		197	1.20	2.67	1.02	1.01	0.99
		15	1.21	2.69	1.00	1.00	0.98
$[Fe(DHBQ)(H_2O)_2]_n$	9	295[e]	1.16	1.47	1.03	1.01	0.98
		295[f]	0.38	0.83	0.76	0.48	0.64
		15[e]	1.21	1.49	1.01	1.00	0.99
		15[f]	0.41	0.84	0.92	0.61	0.79
$[Fe(CA)(pyr)]_n$	9	295	1.02	2.36	0.98	0.96	0.97
		120	1.12	2.81	0.99	0.99	1.00
		18	1.21	3.09	0.96	0.98	1.03
$[Fe(DHBQ)(pyr)]_n$	9	295	1.12	2.31	0.99	0.97	0.96
		77	1.16	2.46	1.00	1.01	0.99
		20	1.19	2.71	1.00	1.02	1.02
$Fe_2(CA)_3(H_2O)_4 \cdot 4H_2O$	8	295	0.40	0.80	1.28	0.77	0.60
		230	0.41	0.81	1.19	0.81	0.63
		175	0.45	0.80	1.30	0.94	0.65
		100	0.48	0.84	1.27	1.01	0.71
		77	0.50	0.82	1.39	1.04	0.74
		40	0.49	0.85	1.27	1.03	0.80
		15	0.51	0.86	1.19	0.97	0.87
$Fe_2(DHBQ)_3(H_2O)_4$	25	295	0.40	0.77	0.86	0.84	0.96
		201	0.42	0.77	0.88	0.85	0.98
		144	0.46	0.78	0.81	0.78	0.98
		50	0.47	0.78	0.90	0.89	1.00
		15	0.49	0.77	0.93	0.89	0.95
	8	295	0.44	0.78	0.86	0.69	0.57
		200	0.45	0.81	0.86	0.73	0.61
		115	0.45	0.80	0.88	0.79	0.70
		77	0.46	0.79	0.85	0.79	0.75
		50	0.47	0.80	0.83	0.80	0.86
		15	0.49	0.80	0.84	0.80	0.95

[a] Data (relative to natural α-Fe foil) obtained for samples dispersed in Vaseline. [b] Full-

width at half maximum ratio for line at higher velocity (2) to line at lower velocity (1). [c] Area ratio. [d] Line intensity ratio (corrected for parabolic baseline). [e] Fe(II) site. [f] Fe(III) site.

Table IV. Thermal Weight Loss Data[a]

Compd	T,°C [b]	Weight Loss, % [c] obsd	calcd
$Fe_2(CA)_3(H_2O)_4 \cdot 4H_2O$	100	9.4	8.2
	220	9.4	8.2
	~380	70.6	70.8
$Fe_2(DHBQ)_3(H_2O)_4$	240	12.0	12.1
	~370	70.0	69.3
$[Fe(CA)(H_2O)_2]_n$	250	11.6	12.1
$[Fe(DHBQ)(H_2O)_2]_n$	240	16.0	15.7
$[Fe(CA)(pyr)]_n$	300-400	80.6	83.7
$[Fe(DHBQ)(pyr)]_n$	300-400	80.2	79.6

[a] Obtained in air. [b] Temperature of inflection for the process. [c] % weight loss for the single process.

References and Notes

(1) R. S. Bottei and J. T. Fangman, J. Inorg. Nucl. Chem., 28, 1259 (1966).

(2) R. S. Bottei and D. L. Green, J. Inorg. Nucl. Chem., 30, 1469 (1968).

(3) A. M. Talati and V. N. Mistry, Indian J. Chem., 11, 296 (1973).

(4) D. K. Cabbiness and E. S. Amis, Bull. Chem. Soc. Jpn., 40, 435 (1967).

(5) A. M. Talati and V. N. Mistry, J. Indian Chem. Soc., 50, 225 (1973).

(6) H. Stone, A. B. Robertson, and M. T. Tetenbaum, U. S. Pat. No. 3812066 (1973).

(7) S. Kanda and Y. Saito, Bull. Chem. Soc. Jpn., 30, 192 (1957).

(8) H. Kobayaski, T. Haseda, E. Kanda, and S. Kanda, J. Phys. Soc. Jpn., 18, 349 (1963).

(9) C. Yoshimura, H. Noguchi, T. Inoue, and H. Hara, Bunseki Kagaku, 15, 918 (1966).

(10) N.A.A. Beg, Pak. J. Sci. Ind. Res., 14, 452 (1971).

(11) C. G. Pierpont, L. C. Francesconi, and D. N. Hendrickson, Inorg. Chem., 16, 2367 (1977).

(12) O. N. Kraschka, O. L. Atovmyan, and V. A. Avilov, Tezisy Dokl. - Vses Chugaevskoe Soveshch. Khim. Kompleksn. Soedin., 12th, 2, 244 (1975).

(13) D. K. Cabbiness, E. S. Ames, and K. C. Jackson , J. Chem. Eng. Data, 12, 90 (1967).

(14) The design of this particular Faraday balance incorporates a model CS-202 Displex cryogenic refrigerator manufactured by Air Products and Chemicals Inc, Allentown, PA 18103. This refrigerator operates on a helium cycle to achieve an ultimate temperature of 10K. In order to eliminate vibration introduced by the Displex expander piston, an air-tight PVC membrane separated the electrobalance assembly from the expander. In this way noise levels due to Displex vibration were reduced to less than 10 μg.

(15) D. B. Brown, V. H. Crawford, J. W. Hall, and W. E. Hatfield, J. Phys. Chem. 81, 1303 (1977).

(16) F. E. Mabbs and D. J. Machin, "Magnetism and Transition Metal Complexes", Chapman and Hall, London, 1973, p 5.

(17) See, for example, S. N. Deming and S. L. Morgan, Anal. Chem., 45, 278A (1973) and references therein.

(18) Standard error = $\{\sum_{i=1}^{n} [\mu_{eff}(obs)_i - \mu_{eff}(calcd)_i]^2/(n-k)\}^{1/2}$ where n = no. of data points and k = no. of fitting parameters. A. P. Ginsberg, R. L. Martin, R. W. Brookes, and R. C. Sherwood, Inorg. Chem. , 11, 2884 (1972).

(19) C. W. Allen and D. B. Brown, Inorg. Chem., 13, 2020 (1974).

(20) J. T. Wrobleski, Doctoral Dissertation, University of Missouri-Rolla, 1977.

(21) J. T. Wrobleski and G. J. Long, Appl. Spectrosc., 31, 177 (1977).

(22) Supplementary material.

(23) B. N. Figgis, "Introduction to Ligand Fields", Interscience, New York, N.Y., 1966, p 280.

(24) J. T. Wrobleski and D. B. Brown, unpublished results.

(25) J. T. Wrobleski and D. B. Brown, Inorg. Chem., 17, 0000 (1978).

(26) J. A. Thich, C. C. Ou, D. Powers, B. Vasiliou, D. Mastropaolo, J. A. Potenza, and H. J. Schugar, J. Am. Chem. Soc., 98, 1425 (1976).

(27) W. M. Reiff, W. A. Baker, Jr., and N. E. Erickson, J. Am. Chem. Soc., 90, 4794 (1968).

(28) A. V. Khedekar, J. Lewis, F. E. Mabbs, and H. Weigold, J. Chem. Soc., London, 1561 (1967).

(29) T. R. Felthouse, E. J. Laskowski, and D. N. Hendrickson, Inorg. Chem., 16, 1077 (1977).

(30) B. N. Figgis, J. Lewis, F. E. Mabbs, and G. A. Webb, J. Chem. Soc. A, 442 (1967).

(31) Ref. 16, p 131.

(32) See, for example, J. N. McElearney, Inorg. Chem., 15, 823 (1976), R. Dingle, M. E. Lines, and S. L. Holt, Phys. Rev., 187, 643 (1969), and J. N. McElearney, Inorg. Chem., 17, 248 (1978).

(33) S. Katsura, Phys. Rev., 127, 1508 (1962) and M. E. Fisher, J. Math. Phys., 4, 124 (1963).

(34) Certain inadequacies in the Ising model for the present purpose are well documented. See for example R. W. Jotham, J. Chem. Soc., Chem. Commun., 178 (1973).

(35) M. Habenschuss and B. C. Gerstein, J. Chem. Phys., 61, 852 (1974).

(36) A. Santoro, A. D. Mighell, and C. W. Reimann, Acta Crystallogr. B, 26, 979 (1970).

(37) S. A. Adeyemi, E. C. Johnson, F. J. Miller, and T. J. Meyer, Inorg. Chem., 12, 2371 (1973).

(38) P. W. Carreck, M. Goldstein, E. M. McPartlin, and W. D. Unsworth, J. Chem. Soc., Chem. Commun., 1634 (1971).

(39) D. B. Losee, H. W. Richardson, and W. E. Hatfield, J. Chem. Phys., 59, 3600 (1973).

(40) Unless otherwise stated, Mössbauer parameters presented herein have the following maximum uncertainties: δ, ± 0.03 mm/s; ΔE_Q, ± 0.03 mm/s; Γ_2/Γ_1, ± 0.08; A_2/A_1, ± 0.08; I_2/I_1, ± 0.04.

(41) R. V. Pound and G. A. Rebka, Jr., Phys. Rev. Letters, 4, 274 (1960) and B. D. Josephson, Phys. Rev. Letters, 4, 341 (1960).

(42) See for example N. N. Greenwood and T. C. Gibb, "Mössbauer Spectroscopy", Chapman and Hall, London, 1971, pp 66-77.

(43) V. I. Goldanskii and E. F. Makarov, "Chemical Applications of Mössbauer Spectroscopy", V. I. Goldanskii and R. H. Herber, Ed., Academic Press, New York, 1968, pp 102-107.

(44) T. C. Gibb, R. Greatrex, and N. N. Greenwood, J. Chem. Soc. A, 890 (1968).

(45) The symmetric pyrazine stretch near 1600 cm^{-1} is ir inactive for bidentate pyrazine. M. Goldstein and W. D. Unsworth, Spectrochim. Acta A, 27, 1055 (1971).

Figure Captions

Figure 1. Corrected molar paramagnetic susceptibility ($\bar{\chi}_M$, cgsu) and effective magnetic moment per iron ($\bar{\mu}_{eff}$, μ_B) vs. temperature for $Fe(CA)_3(H_2O)_4 \cdot 4H_2O$. The solid curve is a fit to the HDVV $\underline{S}_1 = \underline{S}_2 = 5/2$ dimer model with $J = -0.95$ cm^{-1}, $g = 2.00$, and $N\alpha = 0.0$.

Figure 2. Corrected molar paramagnetic susceptibility ($\bar{\chi}_M$, cgsu) and effective magnetic moment per iron ($\bar{\mu}_{eff}$, μ_B) vs. temperature for $Fe_2(DHBQ)_3(H_2O)_4$. The solid curve is a fit to the HDVV $\underline{S}_1 = \underline{S}_2 = 5/2$ dimer model with $J = -2.00$ cm^{-1}, $g = 2.00$, and $N\alpha = 0.0$.

Figure 3. Corrected molar paramagnetic susceptibility ($\bar{\chi}_M$, cgsu) and effective magnetic moment per iron ($\bar{\mu}_{eff}$, μ_B) vs. temperature for $[Fe(DHBQ)(H_2O)_2]_n$. The solid curve is a fit to the $\underline{S} = 2$ Heisenberg linear chain model with $J = -1.35$ cm^{-1}, $g = 2.14$, and $N\alpha = 55 \times 10^{-6}$ cgsu.

Figure 4. Corrected molar paramagnetic susceptibility ($\bar{\chi}_M$, cgsu) and effective magnetic moment per iron ($\bar{\mu}_{eff}$, μ_B) vs. temperature for $[Fe(DHBQ)(pyr)]_n$. The solid curve is a fit to the $\underline{S} = 2$ Heisenberg linear chain model with $J = -2.55$ cm^{-1}, $g = 2.14$, $N\alpha = 55 \times 10^{-6}$ cgsu.

Figure 5. Corrected molar paramagnetic susceptibility ($\bar{\chi}_M$, cgsu) and effective magnetic moment per iron ($\bar{\mu}_{eff}$, μ_B) vs. temperature for $[Fe(CA)(pyr)]_n$. The solid curve is a fit to the $\underline{S} = 2$ Heisenberg linear chain model with $J = -0.54$ cm^{-1}, $g = 2.14$, and $N\alpha = 25 \times 10^{-6}$ cgsu.

Figure 6. Room temperature Mössbauer spectrum of $[Fe(CA)(H_2O)_2]_n$. The solid curve is a fit to the parameters given in Table III.[22] 8 mg Fe/cm^2.

Figure 7. Room temperature Mössbauer spectrum of $[Fe(DHBQ)(H_2O)_2]_n$. The solid curve is a fit to the parameters given in Table III.[22] 9 mg Fe/cm^2.

Figure 8. Mössbauer spectra of $[Fe(CA)(pyr)]_n$: A = 295K and B = 18K. The solid curve in A is obtained for a single quadrupole doublet with parameters given in Table III.[22] Spectrum B contains an additional line at 1.0 mm/s. 9 mgFe/cm^2.

Figure 9. Mossbauer spectra of $Fe_2(DHBQ)_3(H_2O)_4$ taken at 295, 77, and 15K. The solid curves represent fits to two lines with parameters given in Table III.[22] 8 mg Fe/cm^2.

Figure 10. Plots of full-width at half maximum ratio (Γ_2/Γ_1), isomer shift (δ,mm/s), area ratio (A_2/A_1), and intensity ratio ($\underline{I}_2/\underline{I}_1$) vs. temperature for the quadrupole doublet of $Fe_2(DHBQ)_3(H_2O)_4$. Open circles (0) refer to data obtained for a "thick" absorber (~ 25 mg Fe/cm^2). Full circles ( ) refer to data obtained for a "thin" absorber (~ 8 mg Fe/cm^2).

Figure 11. Plots of full-width at half maximum ratio (Γ_2/Γ_1), isomer shift (δ,mm/s), area ratio (A_2/A_1), and intensity ratio ($\underline{I}_2/\underline{I}_1$) vs. temperature for the quadrupole doublet of $Fe_2(CA)(H_2O)_4 \cdot 4H_2O$.

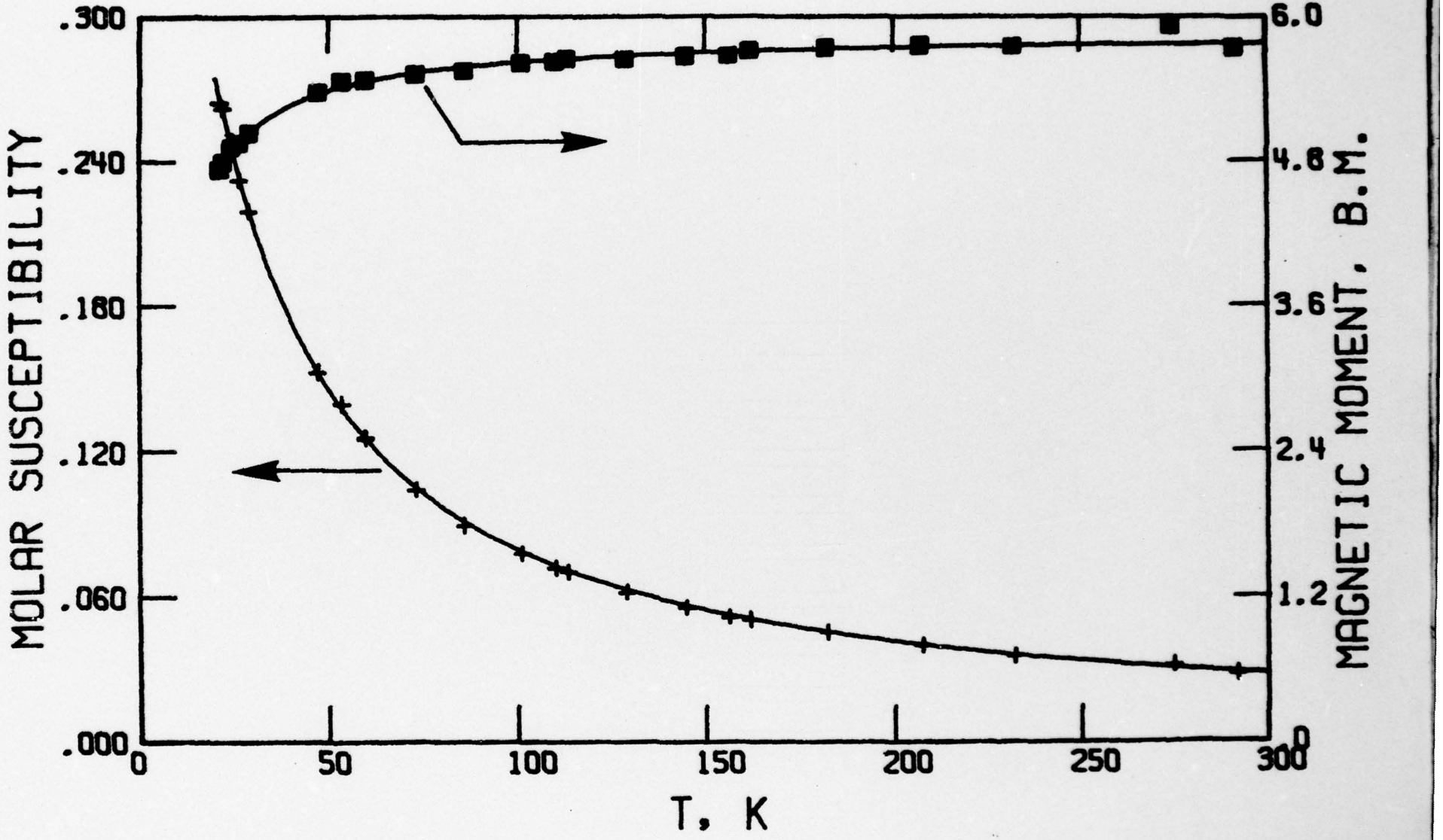
.300
.240
.180
.120
.060
.000
MOLAR SUSCEPTIBILITY
6.0
4.8
3.6
2.4
1.2
0
MAGNETIC MOMENT, B.M.
0
50
100
150
200
250
300
T, K

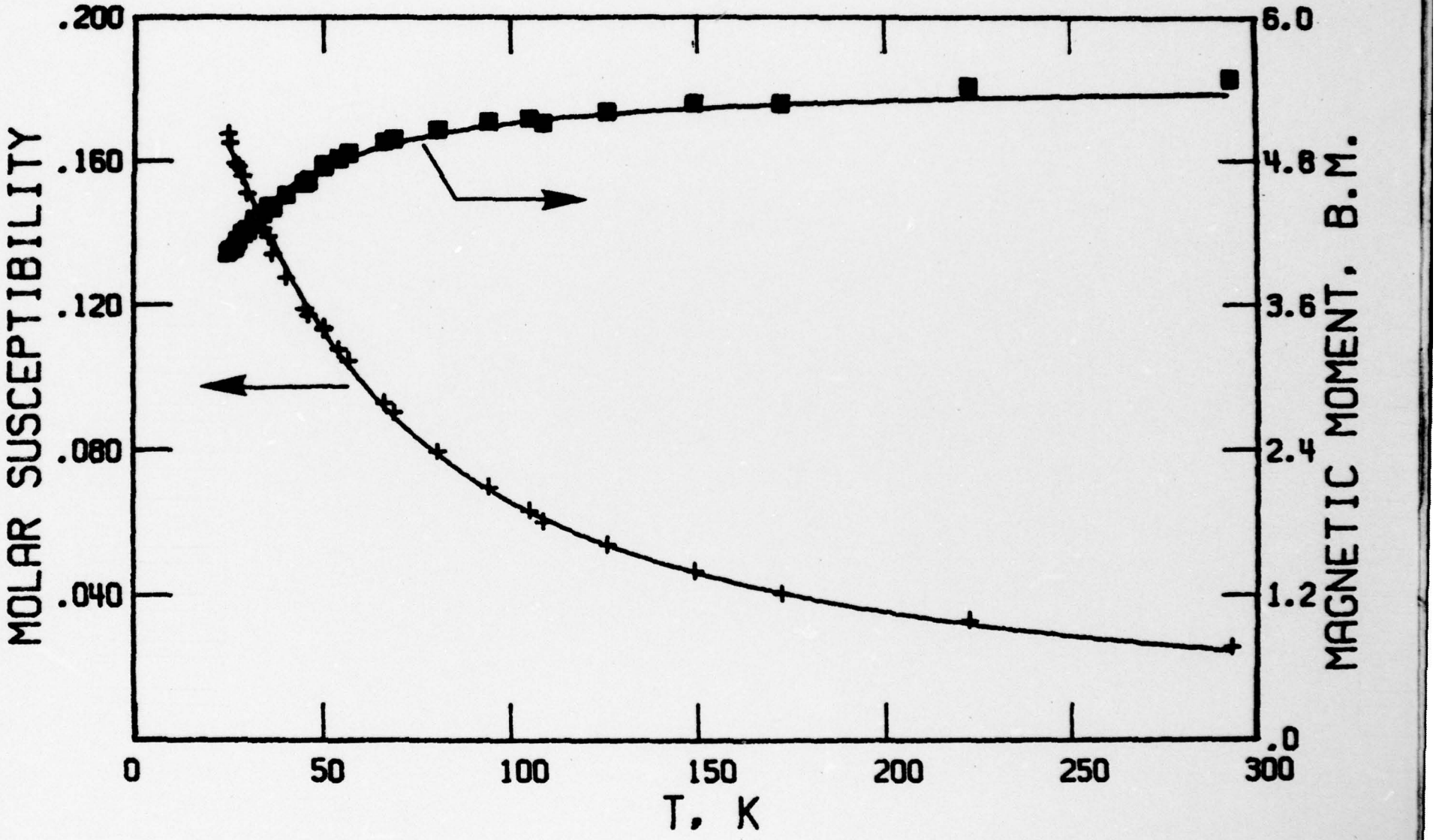
.200
.160
.120
.080
.040
MOLAR SUSCEPTIBILITY
6.0
4.8
3.6
2.4
1.2
.0
MAGNETIC MOMENT, B.M.
0
50
100
150
200
250
300
T, K

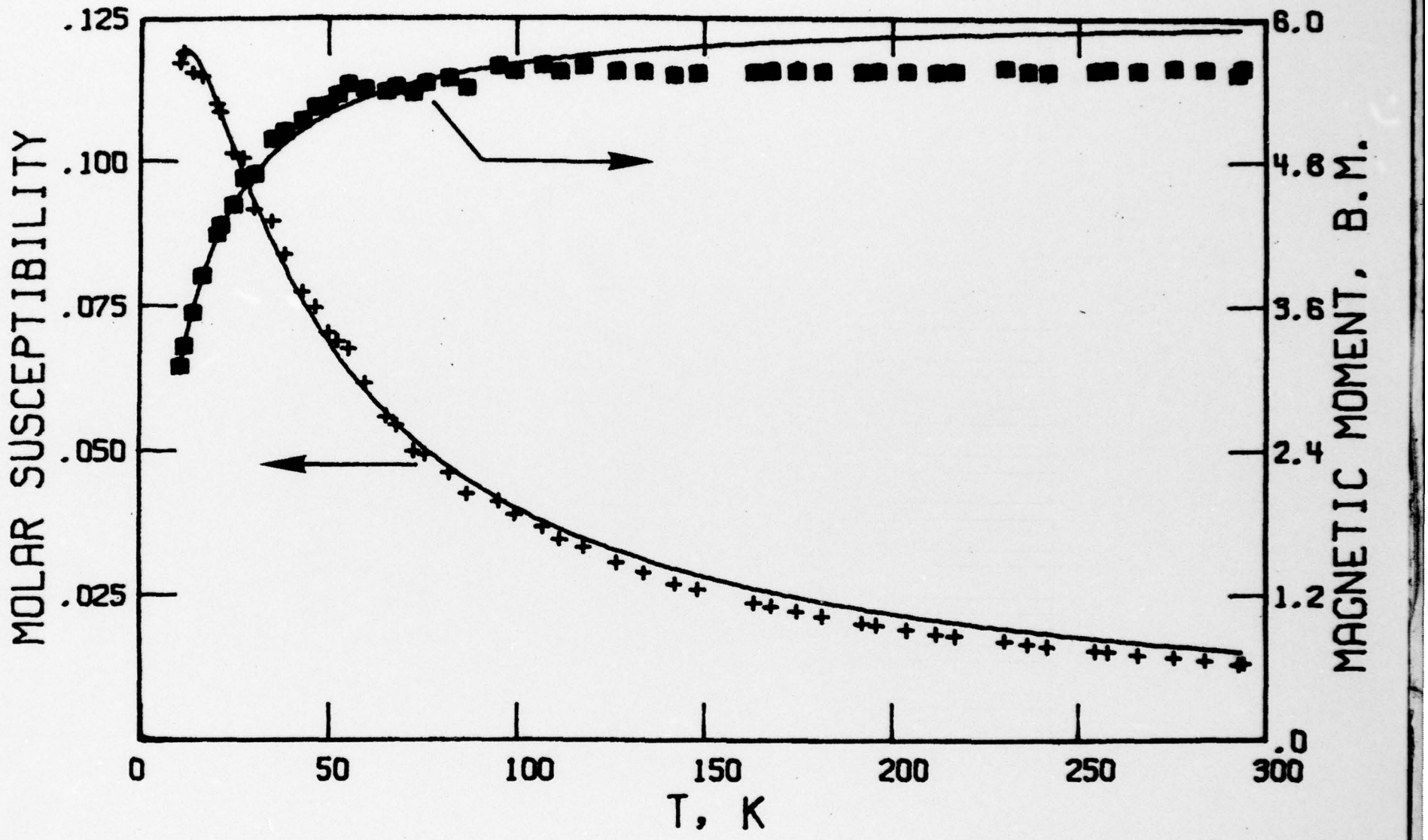
.125
.100
.075
.050
.025
MOLAR SUSCEPTIBILITY
6.0
4.8
3.6
2.4
1.2
.0
MAGNETIC MOMENT, B.M.
0
50
100
150
200
250
300
T, K

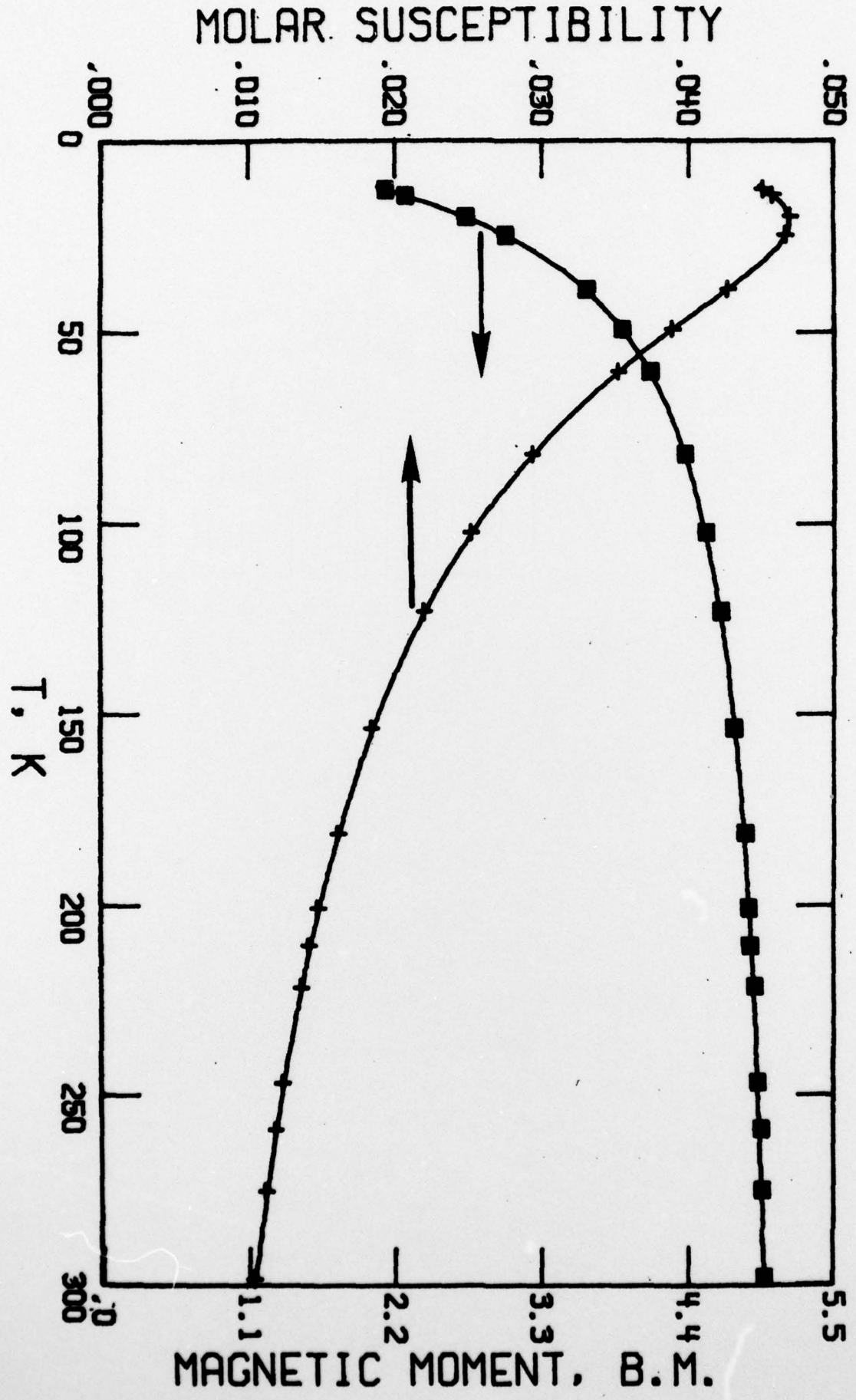
MOLAR SUSCEPTIBILITY
.000
.010
.020
.030
.040
.050
0
50
100
150
200
250
300
T, K
0.0
1.1
2.2
3.3
4.4
5.5
MAGNETIC MOMENT, B.M.

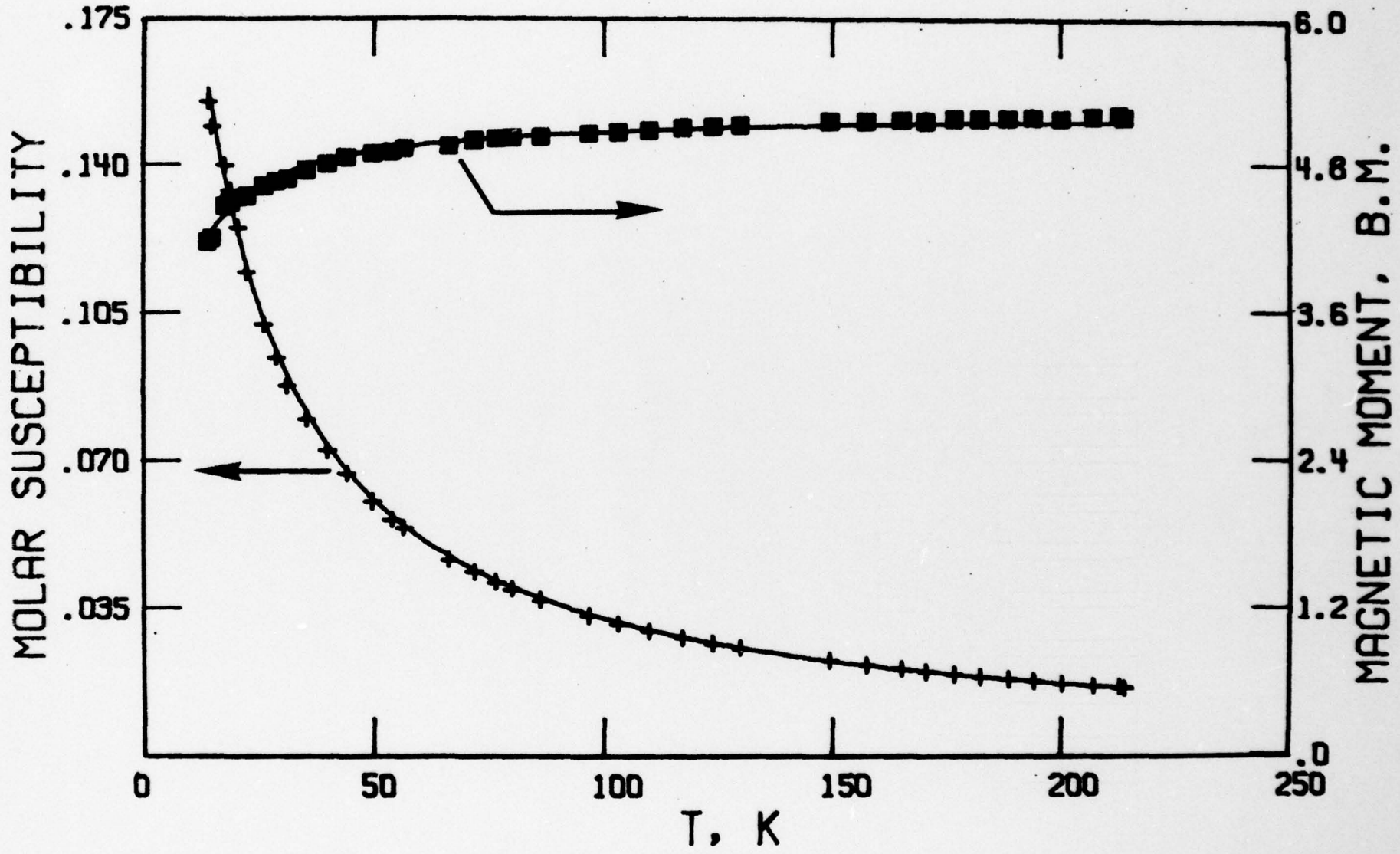
.175
.140
.105
.070
.035
MOLAR SUSCEPTIBILITY
6.0
4.8
3.6
2.4
1.2
.0
MAGNETIC MOMENT, B.M.
0
50
100
150
200
250
T, K

RELATIVE % TRANSMISSION
85.6
89.2
92.8
96.4
100.0
SOURCE VELOCITY, MM/S
-5
-4
-3
-2
-1
0
1
2
3
4
5
6

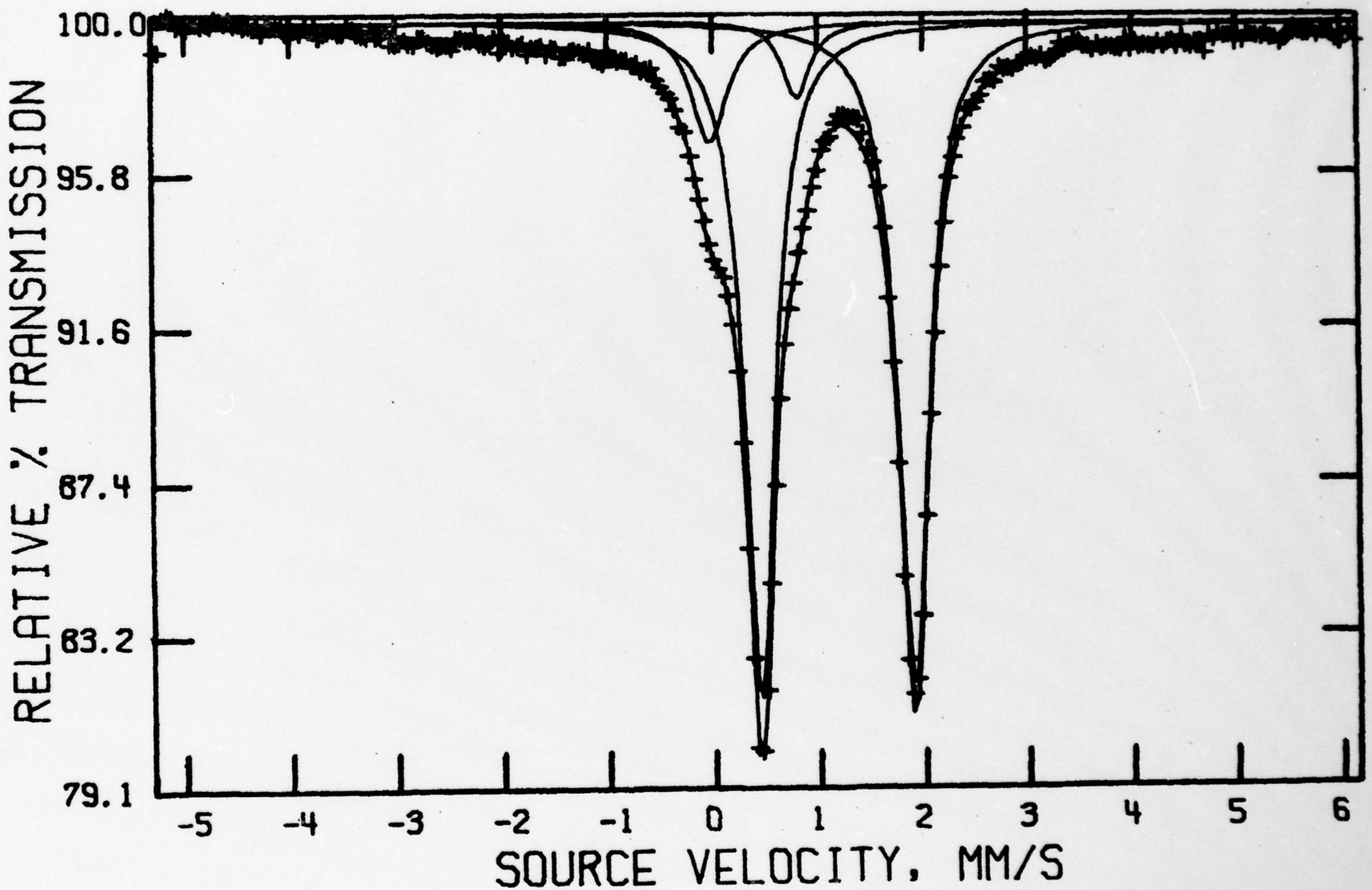
100.0
95.8
91.6
87.4
83.2
79.1
RELATIVE % TRANSMISSION
-5
-4
-3
-2
-1
0
1
2
3
4
5
6
SOURCE VELOCITY, MM/S

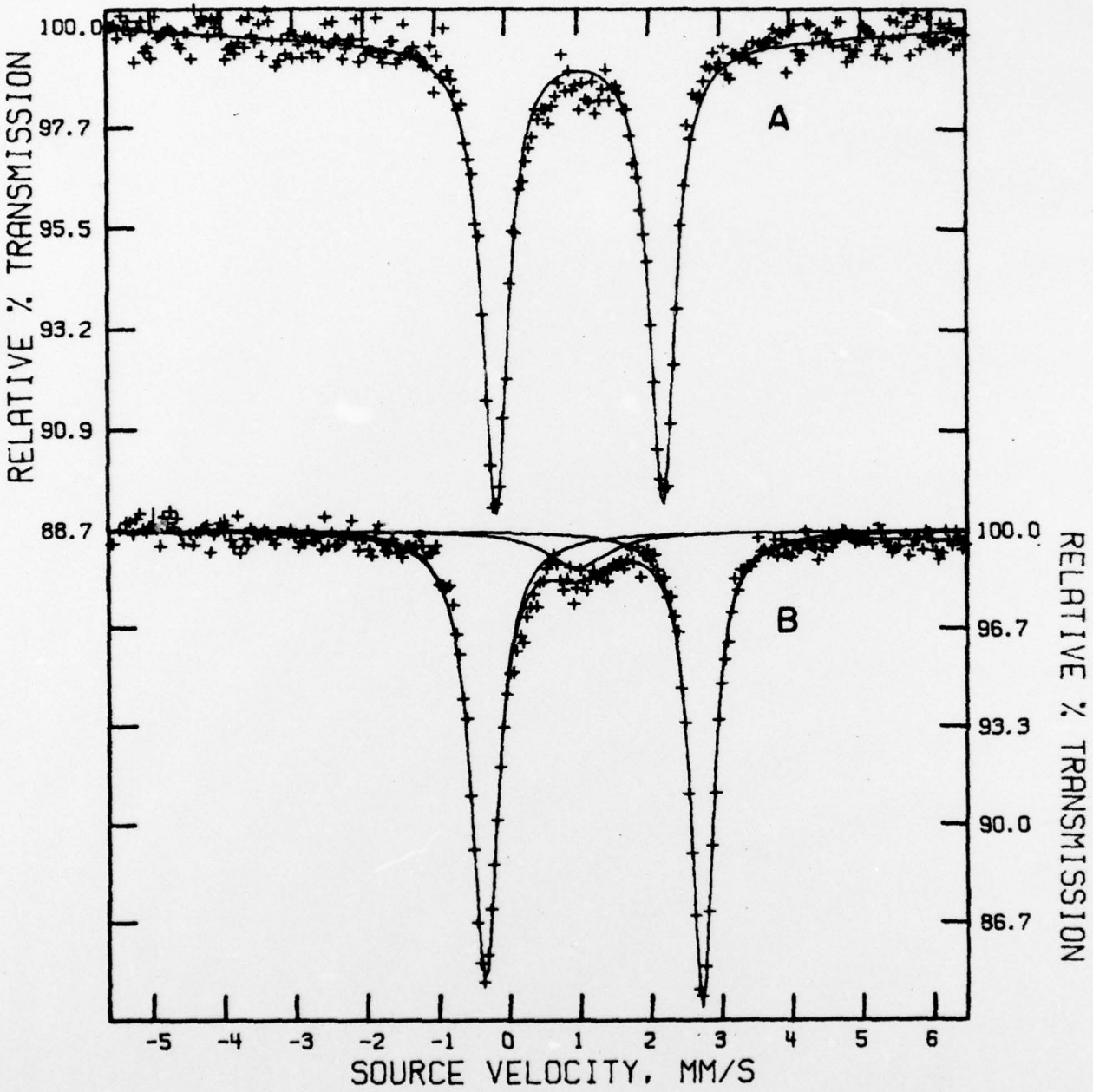
RELATIVE % TRANSMISSION
100.0
97.7
95.5
93.2
90.9
88.7
A
B
100.0
96.7
93.3
90.0
86.7
RELATIVE % TRANSMISSION
-5
-4
-3
-2
-1
0
1
2
3
4
5
6
SOURCE VELOCITY, MM/S

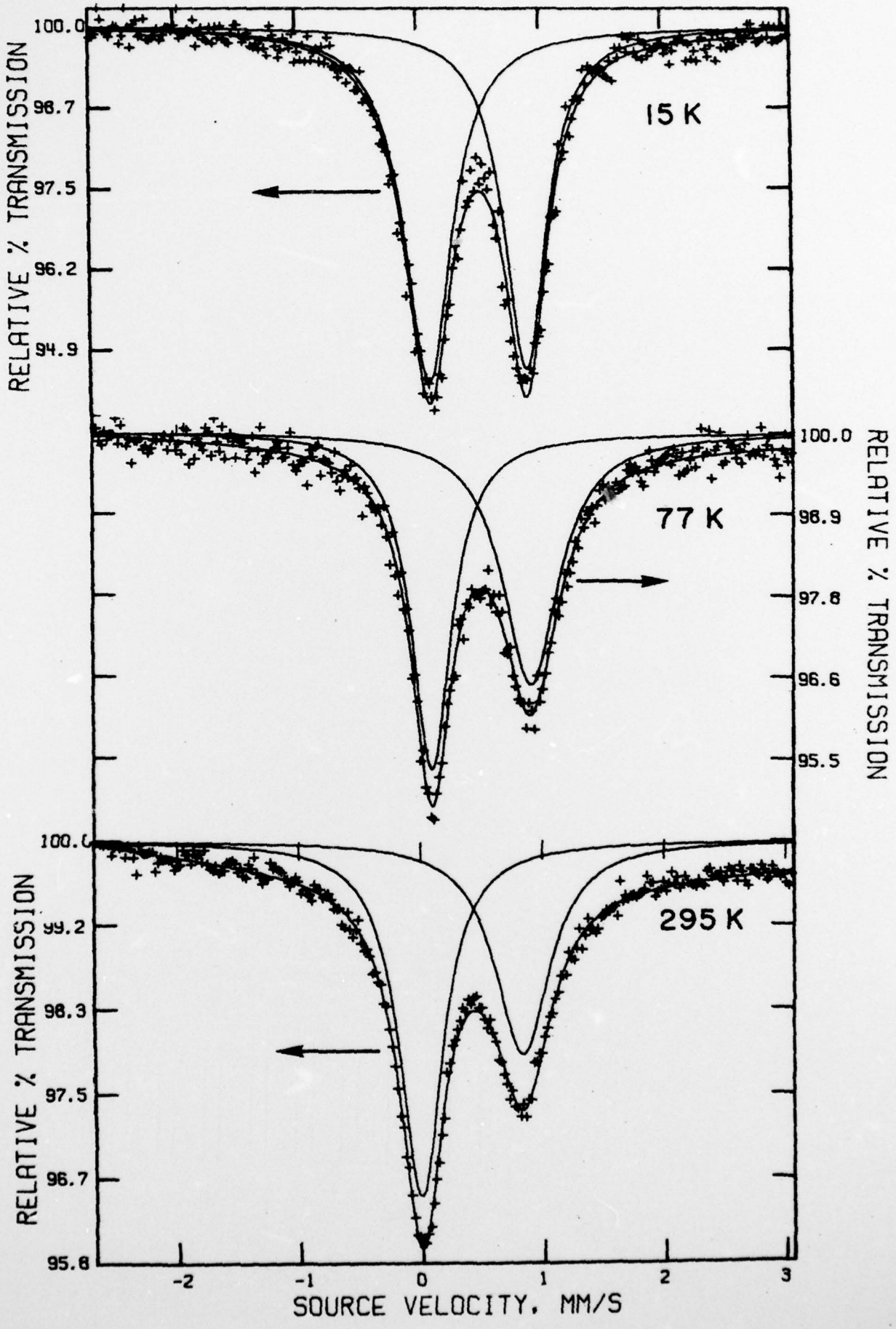
15 K
77 K
295 K
RELATIVE % TRANSMISSION
100.0
98.7
97.5
96.2
94.9
96.9
97.8
96.6
95.5
99.2
98.3
97.5
96.7
95.8
-2
-1
0
1
2
3
SOURCE VELOCITY, MM/S

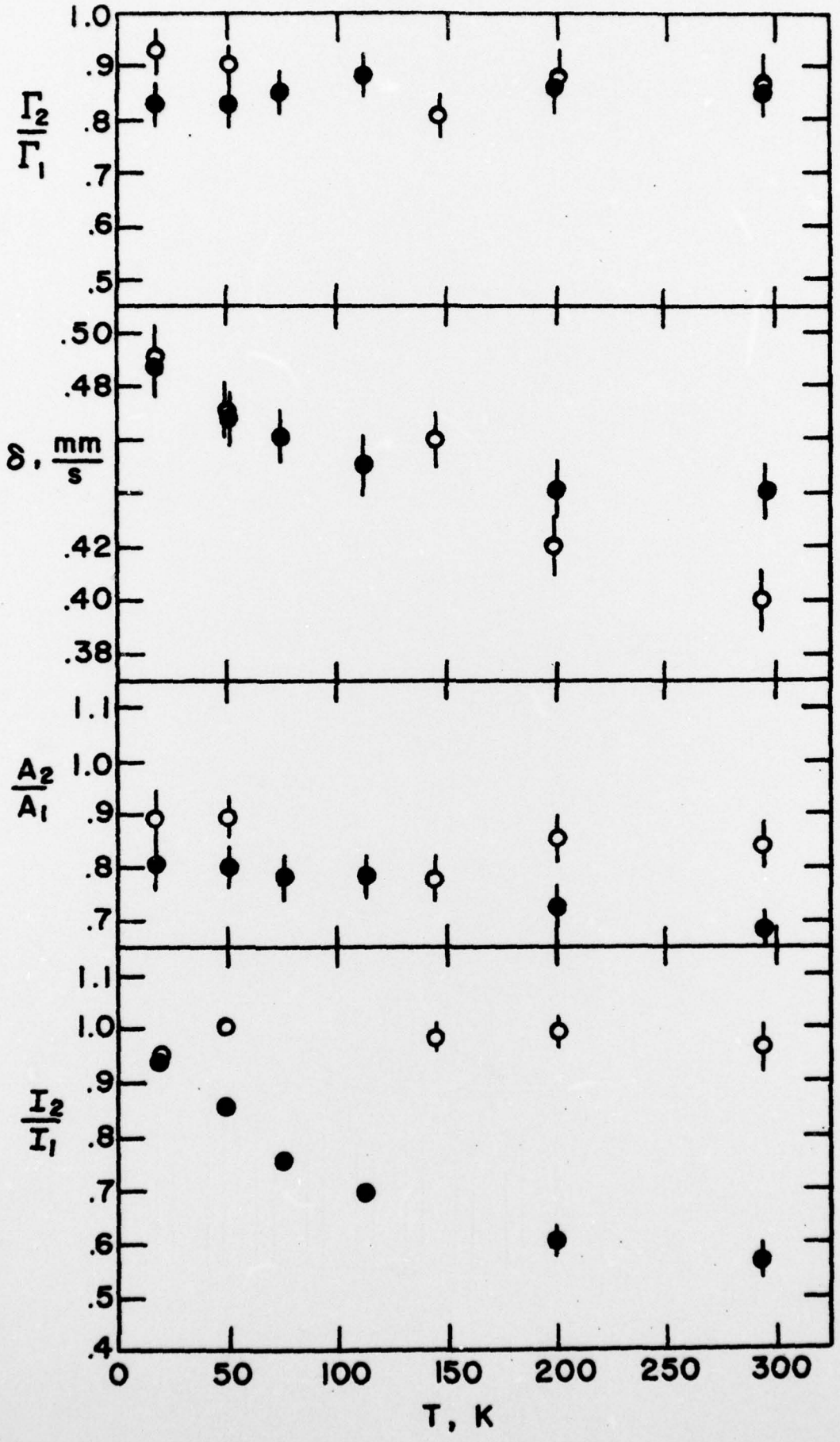
1.0
.9
.8
.7
.6
.5
Γ2/Γ1
.50
.48
.42
.40
.38
δ, mm/s
1.1
1.0
.9
.8
.7
A2/A1
1.1
1.0
.9
.8
.7
.6
.5
.4
I2/I1
0
50
100
150
200
250
300
T, K

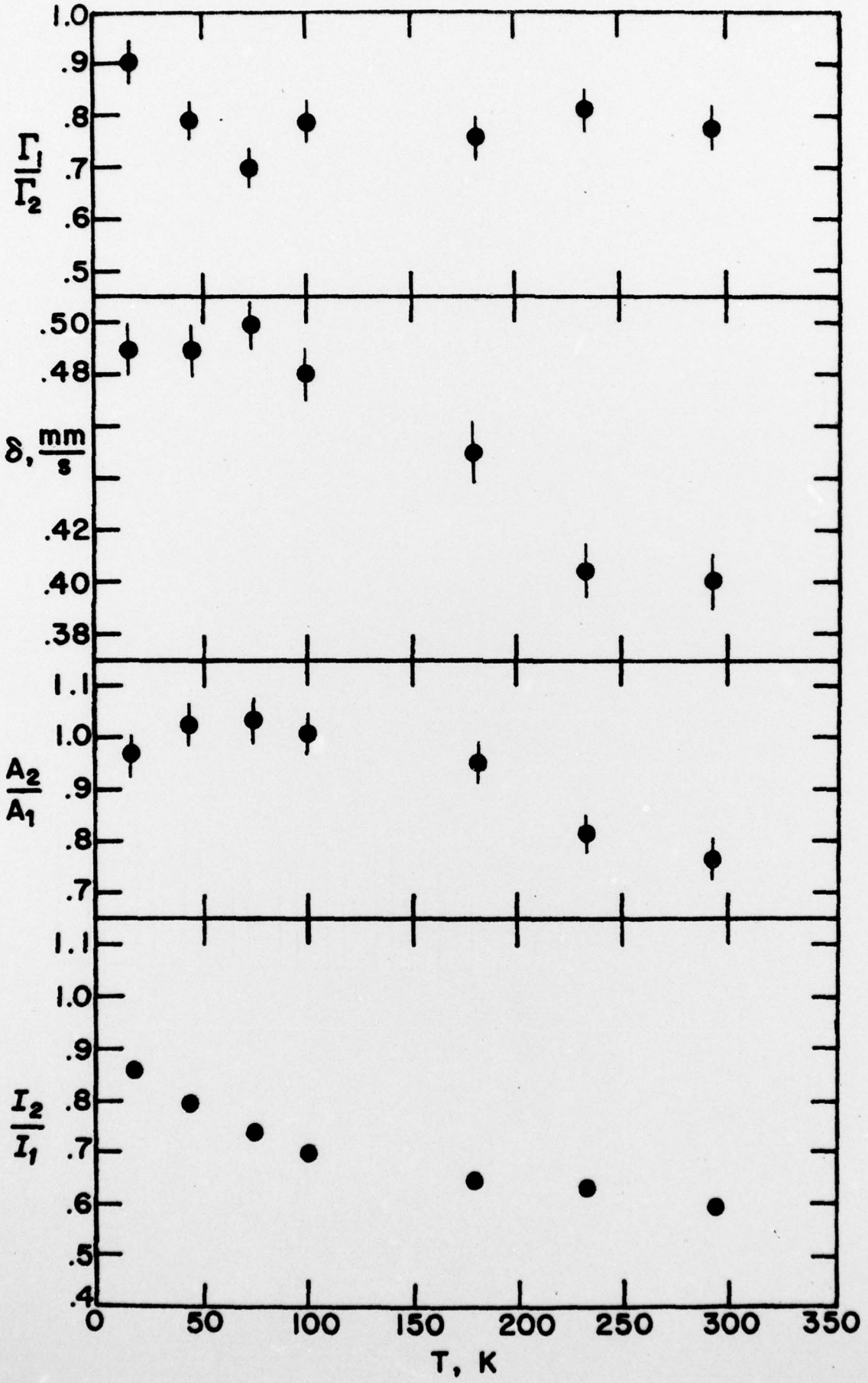
1.0
.9
.8
.7
.6
.5
$\frac{\Gamma_1}{\Gamma_2}$
.50
.48
.42
.40
.38
$\delta, \frac{mm}{s}$
1.1
1.0
.9
.8
.7
$\frac{A_2}{A_1}$
1.1
1.0
.9
.8
.7
.6
.5
.4
$\frac{I_2}{I_1}$
0
50
100
150
200
250
300
350
T, K